UNIVERSIDADE DA BEIRA INTERIOR
Engenharia

Effect of Crossflow Variation on Impacting Droplets

(versão corrigida após defesa)

Filipa Leal Pereira

Dissertação para obtenção do Grau de Mestre em
Engenharia Aeronáutica
(Ciclo de estudos integrado)

Orientador: Prof. Doutor André Resende Rodrigues da Silva

Covilhã, julho de 2019

Acknowledgements

Firstly, I would like to thank my supervisor, Assistant Professor André Resende Rodrigues da Silva, for the opportunity given to develop the present work, for his guidance, dedication and knowledge sharing.

In addition, I would like to thank my colleagues and friends that worked by my side in AEROG. To Inês Ferrão, a special thanks for all the days invested in teaching me and guiding me through the laboratory. To Francisco Carvalho, for being the friend I need. To Daniel Rodrigues, Cátia Moura, Daniela Ribeiro, Emanuel Camacho and Leandro Magalhães for providing me good disposition during this past months of hard work.

To my friends, Elisa Duarte, Sílvia Silva, Flávio Rosa, Bárbara Martins, António Rodrigues, Pedro Nunes, Burcu Dilaver, Pedro Dente and Francisca Garcia for the friendship, support and unforgettable moments through this five year long journey. To Luís Romeiro for the help and amazing moments. You are my example.

I want and must thank my family, especially my parents, Marta and Ernesto, and godparents, Fernando and Maria, for always supporting me in this academic journey. I am eternally grateful for allowing me to follow my dream and for always walking by my side. My brother, Pedro Pereira, for making my life more colourful and happy. You will forever have someone on your corner to protect you and guide you through your life.

Last but not least, thank you with all my heart to Gabriel Carrolo for helping grow and shape the woman that I am today. Your advices, love, affection and happiness made this period of my life the best one yet. Thank you for your patience, support and for boosting my confidence not letting me give up. You will be always treasured.

Resumo

O fenómeno do impacto de gotas tem diversas aplicações na engenharia e processos industriais, como em arrefecimento, pintura e revestimentos por sprays. Em engenharia aeronáutica, impactos de gotas a alta velocidade podem causar erosão em turbinas e o impacto de gotas de combustível nas paredes de motores de combustão interna afeta a razão de evaporação de combustível e a distribuição de gotas. O resultado do impacto de gotas depende das propriedades do líquido, das características superfície de impacto e dos parâmetros cinemáticos.

O uso excessivo de combustíveis fósseis levou o homem a encontrar alternativas viáveis e mais ecológicas, de forma a reduzir emissões nocivas. Desta maneira, o estudo de combustíveis biológicos alternativos torna-se indispensável de forma a compreender o seu comportamento quando aplicados no sector aeronáutico.

Embora estes fenómenos sejam alvo de diversos estudos, estudos envolvendo gotas de Jet A-1 misturadas com NEXBTL são escassas. Assim sendo, um estudo fundamental da influência de um escoamento cruzado no impacto de gotas foi realizado.

Para estudar o comportamento da colisão de gotas em superfícies secas sob o efeito de um escoamento cruzado, foi utilizada uma instalação experimental. O impacto normal foi, também, estudado de forma a melhor compreender a influência da variação escoamento cruzado. Os estudos experimentais foram realizados com velocidades de crossflow de $7m.s^{-1}$,$10m.s^{-1}$, $12m.s^{-1}$ e $15m.s^{-1}$ e com quatro fluídos: 100% Jet-Fuel, 75% JF - 25% HVO, 50% JF - 50% HVO e H_2O (água destilada). Tendo em consideração que a legislação atual para o sector aeronáutico apenas permite uma percentagem mínima em volume de 50% Jet-Fuel, deste modo não foram consideradas outras misturas.

Observou-se que a transição não-splash/splash para o impacto normal de uma gota difere do impacto sob a influência de um escoamento cruzado, onde as componentes da velocidade aparentam ter significância. Assim, os resultados experimentais foram comparados com as correlações empíricas propostas pela literatura. Foi também verificado que um aumento na velocidade tangencial no instante anterior ao impacto, ou seja, correspondendo a uma velocidade do escoamento cruzado maior aparenta reduzir a ocurrência das pequenas gotas secundárias.

Palavras-chave

Impacto de gotas, Jet-Fuel, Biofuel, Escoamento cruzado, Atomização secundária, Transição não-splash/splash, Sprays.

Abstract

The phenomena of droplet impingement has several applications in engineering and industrial processes, such as spray cooling, spray painting and spray coating. For aeronautical engineering, high-speed impacts can cause erosion in steam turbines and the impact of fuel sprays on a wall of internal combustion engines affects the rate of fuel evaporation and droplet distribution. The outcome of droplet impingement depends on the liquid and its properties, the impact surface and kinematic parameters.

The excessive use of fossil fuels led humans to find more ecological viable alternatives, in order to reduce harmful exhaust emissions of liquid-fuel combustors. In this way, the study of biological alternative fuels has proven to be imperative in order to understand its behaviour when employed in the aeronautical sector.

Although these phenomena are widely studied, researches concerning the impact of Jet A-1 mixed with NEXBTL biofuel droplets influenced by a crossflow are scarce. Consequently, a fundamental study of the influence of crossflow variation on impacting droplets is performed.

To study the droplet impingement behaviour on a smooth, dry aluminium surface, an experimental facility was used. Normal impact is studied in order to better understand the influence of the crossflow. The experiments are conducted with crossflow velocities of $7m.s^{-1}$,$10m.s^{-1}$, $12m.s^{-1}$ and $15m.s^{-1}$ and four fluids: 100% Jet-Fuel, 75% JF - 25% HVO, 50% JF - 50% HVO and H_2O (pure water) as reference. Considering that present legislation in the aeronautical sector allows a minimum concentration of 50% Jet-Fuel, no other mixtures are considered.

It was observed that the non-splash/splash transition for normal impact differs from crossflow impact, where both velocity components have effect on impact outcome. Thus, the experimental results were compared with empirical correlations proposed in the literature. It was also verified that an increase of tangential velocity, i.e, an increase in crossflow velocity, smoothed the extent of small secondary droplets.

Keywords

Droplet impact, Jet Fuel, Biofuel, Crossflow, Secondary atomization, Non-splash/splash transition, Sprays.

Contents

List of Figures

List of Tables

Nomenclature

A, B	Surface Roughness Coefficient
a, b, k	Dependent Constants
B	Breakup
Bo	Bond Number
Ca	Capillary Number
D	Deposition
D_0	Droplet Diameter
D_{in}	Needle Inner Diameter
D_{out}	Needle Outer Diameter
Fr	Froude Number
g	Gravitational Constant
K_c	Splashing Parameter
La	Laplace Number
m	Mass of substance
Oh	Ohnesorge Number
Ra	Mean Roughness Surface
Re	Reynolds Number
U	Impact Velocity
U_{cf}	Crossflow Velocity
U_n	Normal Velocity Component
U_t	Tangential Velocity Component
V	Volume of substance
We	Weber number
$\mathrm{We_c}$	Critical Weber number

Greek Symbols

θ	Incident Angle
θ_c	Contact Angle
θ_{static}	Static Contact angle
μ	Dynamic viscosity
ρ	Density
σ	Surface tension
τ	Non-Dimensional Time

Subscripts

0	Related to drop - initial
c	Critical value
cf	Related to Flow - crossflow
in	Inner diameter
out	Outer diameter
n	Normal velocity coordinate
t	Tangential velocity coordinate

Acronyms

ASTM	American Society for Testing and Materials
CI	Crossflow impact
CS	Corona splash
fps	Frames per second
HEFA	Hydroprocessed Esters and Fatty Acids
HSDI	High Speed Direct Injection
HVO	Hydro-processed Vegetable Oil
JF	Jet Fuel
LED	Light Emitting Diode
PS	Prompt splash
NEXBTL	Next Generation Biomass-to-Liquid
NI	Normal impact

Chapter 1

Introduction

This first chapter describes the motivation and objectives underlying the development of this experimental study. The study of sprays and secondary atomization has numerous applications in engineering and industrial processes, such as engine combustion, icing studies, ink jet printing and atomization processes. However, the behaviour of droplets impinging onto dry surfaces in not fully understood. Therefore, a fundamental study of the different phenomena resulting of droplet impingement is important.

Since most of the studies are based on normal impacts and for water based mixtures and ethanol, the behaviour of jet-fuel mixtures for similar conditions and for impacts under the influence of crossflow is different, thus being of paramount importance to be studied and understood.

1.1 Motivation

The desire to fly is intrinsic to man since we looked up to the sky and noticed the birds. Through history many tried, many failed and many succeeded, this was only possible due to the constant desire to advance and improve. Nowadays, the aeronautic sector has proven indispensable to society, in this way, the search for more efficient and ecological fuels is imperative. The dependence on fossil fuels led humanity to a difficult return point, forcing humans to adapt and find ways to reduce its use due to their connection to increasing pollution . The introduction of biofuel mixtures in aero-engines could be a starting point.

Current legislation for the aeronautical sector allows the mixture of conventional jet fuel with HEFA (Hydroprocessed Esters and Fatty Acids) type alternative fuels. This legislation, ASTM D1655 and ASTM D7566 [1, 2], also imposes a minimum percentage in volume of 50% jet fuel. So, the present experimental work studies mixtures with a maximum of 50% biofuel. The biofuel chosen is NEXBTL, an Hydro-processed Vegetable Oil (HVO) where animal biomass is not involved [3].

The phenomena of droplet impingement has many aplications, such as spray cooling, spray painting, inkjet printing, pesticide spraying and engine combustion, where the secondary droplet size and distribution (secondary atomization) are taken in consideration.

Since the atomization of turbulent liquid jets injected into fast moving, subsonic gaseous crossflows is an important application in gas turbines and ramjets, the impact of these fluids will be studied for two conditions: with and without presence of a crossflow, in a way to understand the different behaviour. Also, the experimental results will able the comprehension of the differences between biofuel and conventional Jet A-1 in order to enable its use in aero-engines combustors.

1.2 Objectives

Numerous studies were made in order to understand the droplet impingement phenomena. However, researches contemplating the use of jet fuel and biofuel mixtures allied with the use of crossflow are scarce. Thereby, a proper understanding of droplet impingement mechanisms and dynamics is of importance. To achieve this, these objectives were outlined:

- Visualize the outcomes of droplet impingement for normal impact;
- Visualize the outcomes of droplet impingement for impact under the influence of a crossflow velocity of $7\mathrm{m.s}^{-1}$;
- Visualize the influence of crossflow velocity increase on droplet impact outcomes until the occurrence of breakup;
- Compare the results obtained for splashing threshold for normal impact and impact under the influence of a crossflow velocity of $7\mathrm{m.s}^{-1}$;
- Compare the results obtained for the splashing threshold with empirical correlations proposed in the literature.

1.3 Work Structure

This dissertation is composed of five chapters, including the present one providing an overview of the work order.

The literature contextualization is portrayed in chapter 2 with all of the relevant non-dimensional groups and their physical meaning explained. The various phenomena of droplet impingement are described and the influence of a crossflow is introduced.

Chapter 3 describes the experimental facility and all the components that enable the study of droplet impingement with and without crossflow. Fluid physical properties will also be exposed in this chapter.

Results and discussion can be found in Chapter 4. Firstly, the phenomena visualization results will be presented for normal impact, impact with crossflow and for the crossflow variation study. Following, the results for the threshold will be shown, where the empirical correlations found in the literature are plotted against the results obtained in this experimental work.

Lastly, Chapter 5 summarizes the most important conclusions and suggestions for future studies.

Chapter 2

Literature Review

The phenomena resultant from droplet impingement has many applications such as spray cooling, inkjet printing, pesticide spraying and engine combustion, where the secondary droplet size distribution after impact is taken into consideration.

The outcome of droplet impact on a solid surface depends on the properties of the liquid, the surface conditions and the kinematic parameters, i.e., velocity and momentum, etc. Therefore, there is the need to relate all of these aspects when analysing the impact. Whence, the impinging governing parameters, droplet/wall interactions, influence of a crossflow and deposition/splash transition are addressed in the following subsections.

2.1 Impingement Governing Parameters

As mentioned previously, the phenomena of droplet impingement are conditioned by parameters such as liquid properties (density, viscosity and surface tension) and surface conditions. The major non-dimensional groups governing droplet impact that will be described below include the Weber, Reynolds, Ohnesorge and Bond number. Surface roughness and impact angle are also presented below.

Non-dimensional Numbers

Weber number (We) represents a relation between the droplet kinetic energy and surface energy, where the viscous effects are neglected,

$$We = \frac{\rho U^2 D_0}{\sigma} \quad (2.1)$$

where U, [$\mathrm{m.s^{-1}}$], corresponds to the droplet impact velocity and $\mathrm{D_0}$, [mm], is the droplet diameter. ρ, [$\mathrm{kg.m^{-3}}$], and σ, $\mathrm{N.m^{-1}}$, are the density and the surface tension of the fluid, respectively.

Reynolds number (Re) relates the inertial forces with the viscous forces,

$$Re = \frac{\rho U D_0}{\mu} \quad (2.2)$$

where, μ, [$\mathrm{kg.(m.s)^{-1}}$], is the dynamic viscosity of the fluid.

Ohnesorge number (Oh) describes the relation between capillarity and viscous forces.

$$Oh = \frac{\mu}{\sqrt{\rho \sigma D_0}} = \frac{\sqrt{We}}{Re} \quad (2.3)$$

Capillary number (Ca) relates viscous forces and surface tension forces.

$$Ca = \frac{We}{Re} = \frac{\mu}{\sigma}U \quad (2.4)$$

Laplace number (La) establishes the relation between the surface tension and viscous forces on the liquid.

$$La = \frac{\rho\sigma D_0}{\mu^2} = \frac{Re^2}{We} \quad (2.5)$$

Bond number (Bo) is the relation between the body gravitational forces and surface tension forces.

$$Bo = \frac{\rho g D_0^2}{\sigma} \quad (2.6)$$

where g is the gravitational acceleration constant.

Froude number (Fr) describes the ratio between inertial and gravitational forces, not taking in consideration the viscous effects. This parameter shows if gravity can be neglected.

$$Fr = \frac{U^2}{gD_0} = \frac{We}{Bo} \quad (2.7)$$

If $\mathrm{Fr} \geq 10^2$, gravity effects can be neglected [4].

Impact Angle

The impact angle (θ) represents the angle between the absolute velocity vector of the impinging droplet and the impact surface, Figure 2.1.

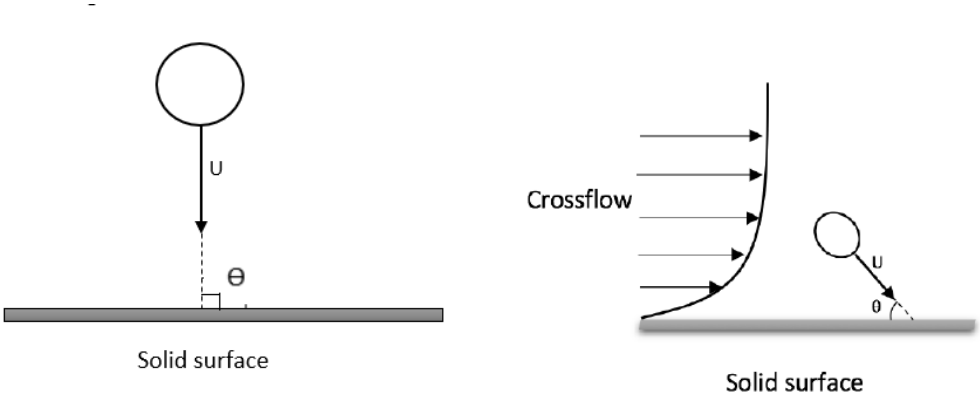

(a) (b)

Figure 2.1: Visual representations of impact angles: a) normal impact, b) impact angle with a crossflow effect adapted from [5].

According to ref. [6], the outcome of an impinging droplet depends largely on the impact angle, which also influences the direction of the secondary droplets for smooth surfaces. Ref.

[7] reported that, if the impact angle is not normal to the impact surface, the tangential velocity component acts to destabilize the spreading liquid film, and hence enhancing droplet fragmentation following its impingement.

It is important to mention that impact angle differs from contact angle (θ_c). According to ref. [8], the contact angle is the angle between the tangent to the droplet profile and the tangent to the surface at the junction point between the air, fluid and solid, as Figure 2.2 shows.

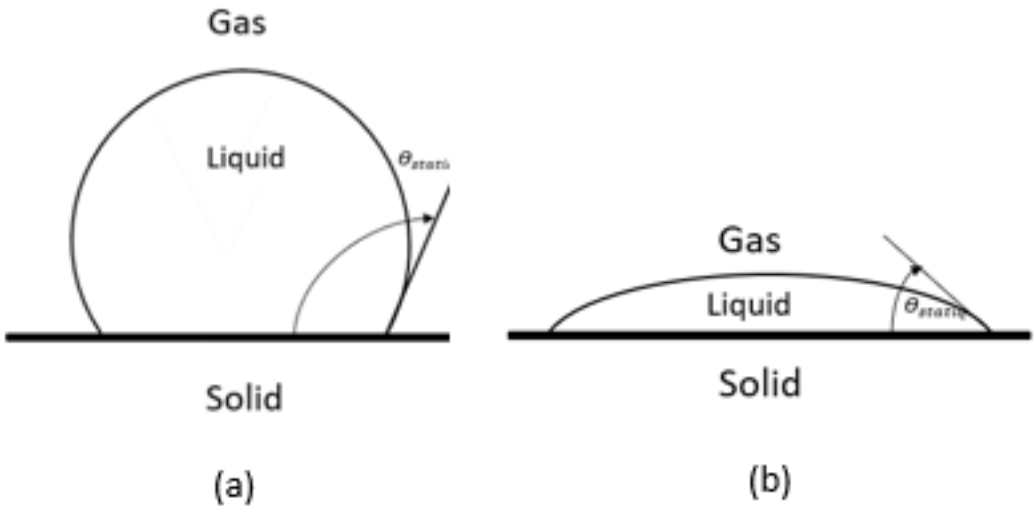

Figure 2.2: Definition of static contact angle: a) Non-wettable system, b) Highly wettable system [9].

In order to understand the concept of contact angle, the wettability concept is explained. Wettability describes the ability of a liquid to spread on a solid surface. It is represented by the angle between the contour of the drop surface and the interface liquid/solid - static contact angle (θ_{static}) - this angle is measured when the droplet is standing on the surface. Contact angles decrease with the increase of wettability.

Surface Roughness

The surface roughness is also an important parameter in droplet impingement dynamics and its normally characterized by its average height [10–13]. Ref. [11] observed that the surface roughness alters the impact angle of impinging droplets, consequently affecting the volume, number, and the size distribution of secondary droplets. For small droplets, this effect becomes more evident. For rough surfaces, the threshold for splash is lowered in comparison to smooth surfaces and the increase of roughness reduces the mass of splash [13, 14]. Ref. [13] reported that the outcome of the impingement not only depends on the kinematic fluid parameters of primary droplets, but also depends on the ratio of the surface roughness compared to the droplet diameter. Therefore, they noticed that the splash phenomena depends on the kinetic energy of the incident droplets, which in term, is independent of the surface properties. If the impact has high kinetic energy and enough momentum normal to the surface to overcome the surface tension of the liquid, splash will appear. Otherwise, if there is low kinetic energy and not enough momentum normal to the surface, the droplet deposits on the surface [11].

2.2 Droplet/Wall Interactions

The behaviour of droplets impinging on dry surfaces is not fully understood. As mentioned above, it depends on a variety of parameters such as the properties of the liquid, the characteristics of the impact surface and exterior influences (crossflow and kinematic parameters).

Considering a droplet impinging on a solid surface, a drop may be spherical or elliptical at the momentum of impact, it can be perpendicular or oblique, in air or vacuum. The liquid may be Newtonian or non-Newtonian, and the surface can be hard or soft, rough or smooth, chemically homogeneous or heterogeneous, porous flat or curved and dry or wet [14], Figure 2.3.

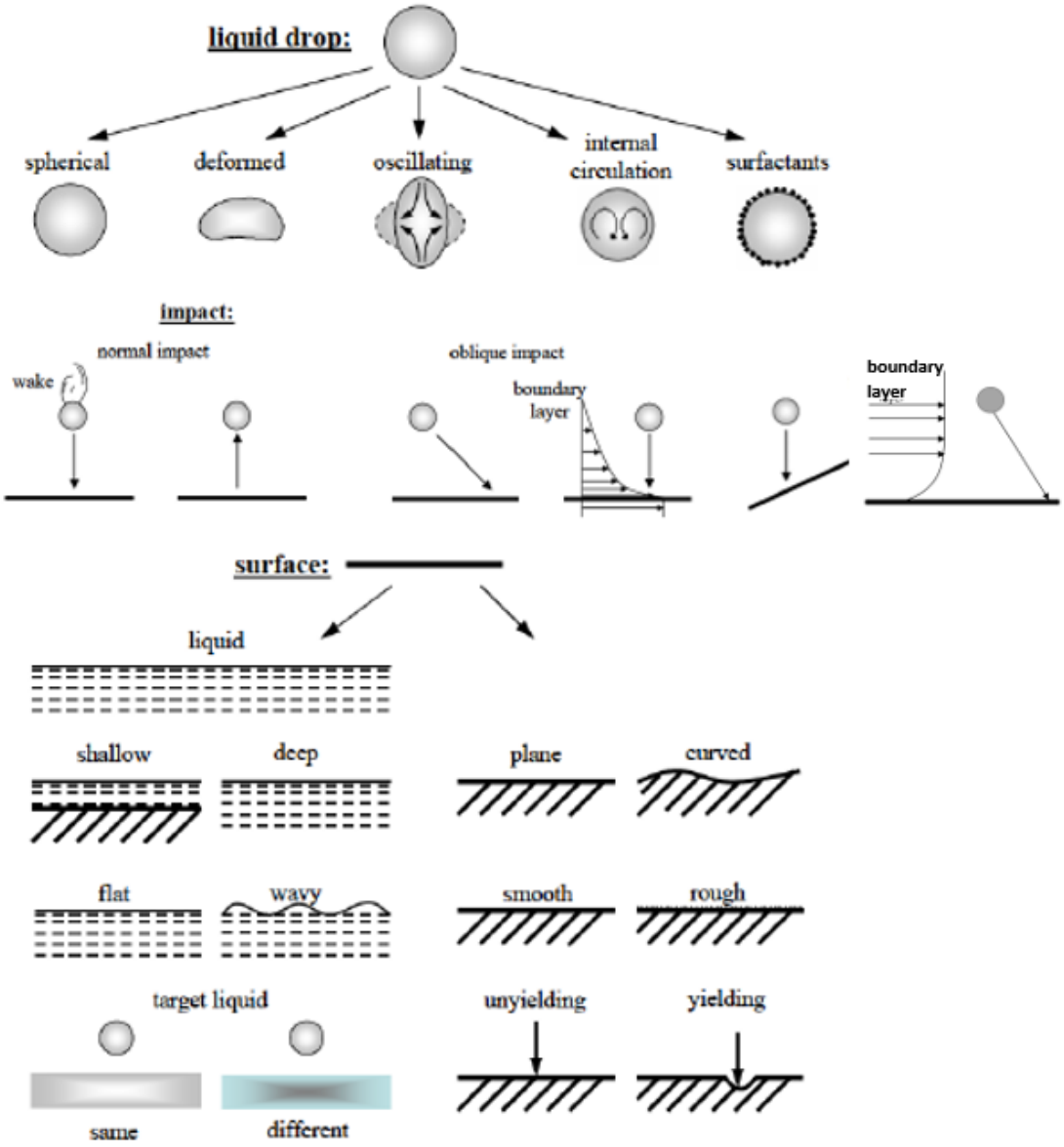

Figure 2.3: Illustration of parameters governing the impact of a liquid drop adapted from [15].

Ref. [16] was one of the firsts to try to understand the impact phenomena but due to technological difficulties was not able to fully advance his study. Ref. [17] identified four main outcomes: stick, rebound, spread and splash. Posteriorly, in their experimental work, ref. [9]

identified six possible outcomes for droplet impact on dry surfaces: spread/deposition, prompt splash, corona splash, receding breakup, partial rebound and complete rebound.

Stick

Stick is when the droplet adheres to the impact wall in nearly spherical form Figure 2.4. This occurs when the impact energy is very low and there is no occurrence of secondary atomization [17].

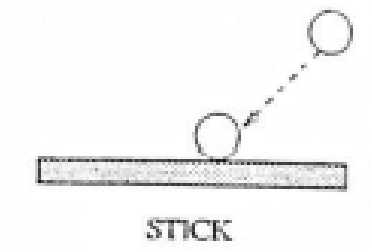

Figure 2.4: Stick regime according to [17].

Spread/Deposition

Spread occurs when the droplet impacts with a moderate velocity, without forming secondary droplets, onto a dry or wetted wall and spreads out to form a wall film for a dry wall, or merges with a pre-existing liquid film for a wetted wall [17].

Deposition refers to an impact in which the droplet spreads out, without forming secondary atomization, and forms a lamella with a visible outer rim. When the lamella reaches the maximum spread diameter it recoils and sticks on the surface [9], Figure 2.5.

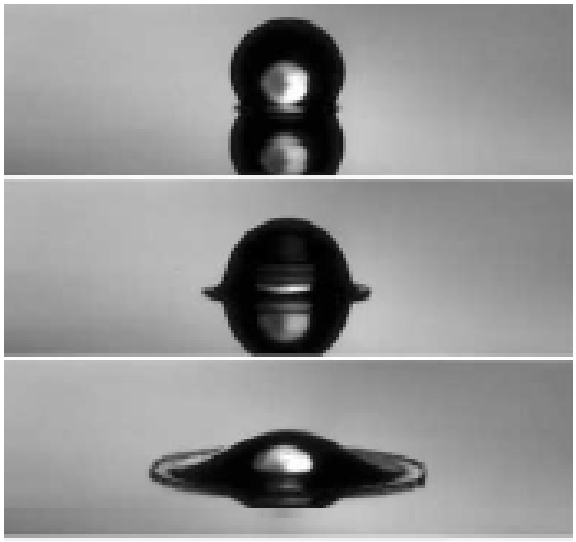

Figure 2.5: Spread/deposition regime adapted from [18].

Splash

Splash occurs when, following the collision of a droplet with a surface at very high impact energy, jets develop on the periphery of the rim. The jets become unstable and breaks into

many fragments (secondary droplets) [17].

Some authors divided this phenomenon in two: prompt and corona splash. Prompt splash occurs for high Weber and Reynolds numbers and the impact generates small droplets that are ejected from the impact region, Figure 2.6.

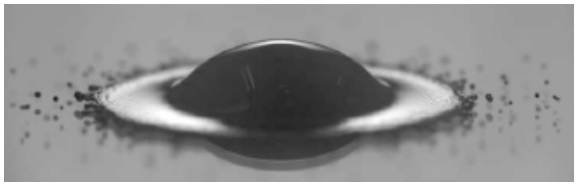

Figure 2.6: Prompt splash regime adapted from [18].

Corona splash, also referred as crown splash, is observed when a drop impacts with sufficient velocity so the outer rim formed by the lamella has enough energy that elevates and creates a crown-like shape. This corona later disintegrates, producing secondary atomization, Figure 2.7.

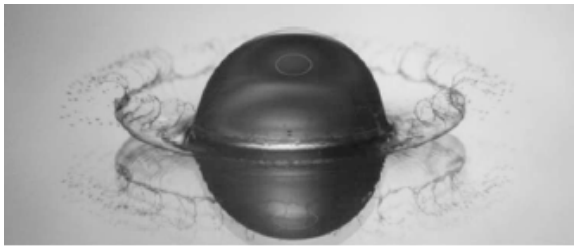

Figure 2.7: Corona splash adapted from [18].

Rebound and Partial Rebound

When the impinging droplet as enough kinetic energy it will bounce off the wall after impact. This is called rebound, Figure 2.8.

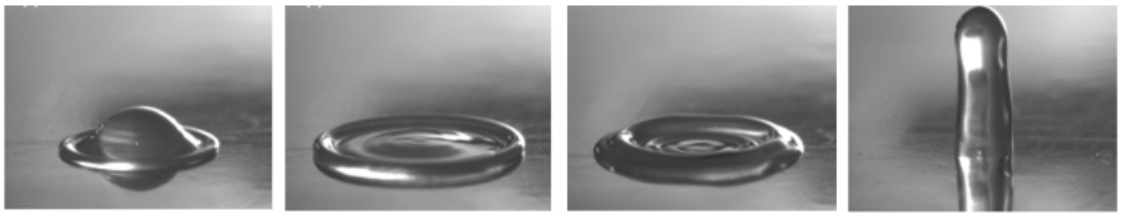

Figure 2.8: Rebound regime adapted from [19].

According to ref. [9], rebound and partial rebound, being dependent on the contact angle and maximum spreading ratio, only occur when a receding phase is observed. For high energy impacts, during the receding phase, not all energy is dissipated and if that energy reaches the impact point the fluid will elevate, Figure 2.9. One of the differences between rebound and partial rebound is found in the dynamic contact angle. For low values a partial rebound occurs and for high values a complete rebound occurs.

(a)

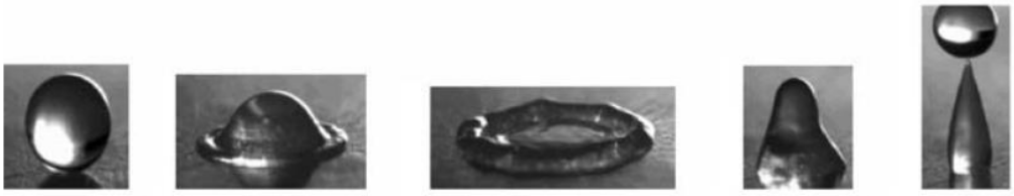

(b)

Figure 2.9: Rebound regime: a) Complete rebound, b) Partial rebound adapted from [9].

Receding Breakup

Receding breakup occurs when the lamella recedes after reaching the maximum spreading ratio and the dynamic contact angle reduces. If it reaches zero, some droplets are left behind by the receding lamella, Figure 2.10.

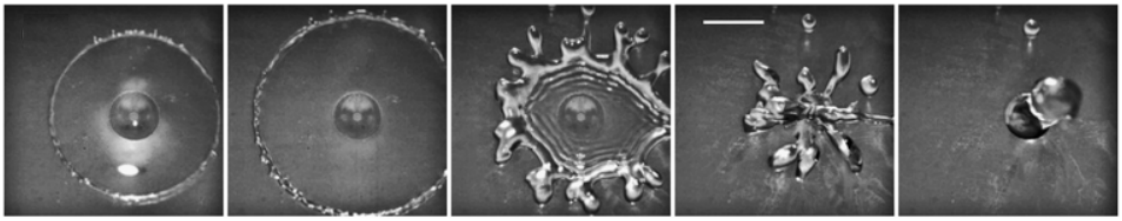

Figure 2.10: Receding breakup regime adapted from [20].

The resultant phenomena of droplet impingement depends on the combination of several conditions, such as the impact velocity, droplet diameter and viscosity. Ref. [9] associated each phenomena with boundary conditions and established the relation in Table 2.1.

Table 2.1: Relation between the six outcomes and boundary conditions adapted from [9].

An increase of	Deposition	Prompt splash	Crown splash	Complete rebound	Partial rebound	Receding breakup
U_0	$\downarrow$	$\uparrow$	$\uparrow$		$\uparrow$	$\uparrow$
D_0	$\downarrow$	$\uparrow$				
σ		$\downarrow$	$\downarrow$	$\uparrow$	$\uparrow$	$\uparrow$
μ	$\uparrow$	$\downarrow$	$\downarrow$			$\downarrow$
θ_{static}				$\uparrow$	$\uparrow$	$\uparrow$

According to ref. [9], an increase of droplets velocity results in a decrease of deposition occurrence and an increase of prompt splash, crown splash, partial rebound and receding breakup occurrence. An increase of droplet initial diameter results in a decrease of deposition occurrence, consequently, the occurrence of prompt splash is increased. For the surface tension, an increase translates to a decrease of splash phenomena occurrence and an increase of rebound and receding breakup phenomena. Regarding the kinematic viscosity, due to its relation with

the velocity parameter, results in a decrease of deposition occurrence and an increase of splash phenomena occurrence. As already mention in the literature, an increase of the static contact angle results in an increase of rebound and receding breakup phenomena.

Fingering is also observed in droplet impingement. The axisymmetric patterns of drop evolution during the kinematic and spreading phases are sometimes perturbed by azimuthal disturbances (e.g. capillary), whose growth results in finger-like shapes at the rim of a spreading drop on a dry wall and is reported by ref. [14], Figure 2.11. Ref. [21] suggested that Rayleigh-Taylor-type instability, i.e., an instability on the interface of two fluids with different densities where the fluid of less density pushes the one with the higher density, leading to fingering could be due to air entrapment under the oncoming drop.

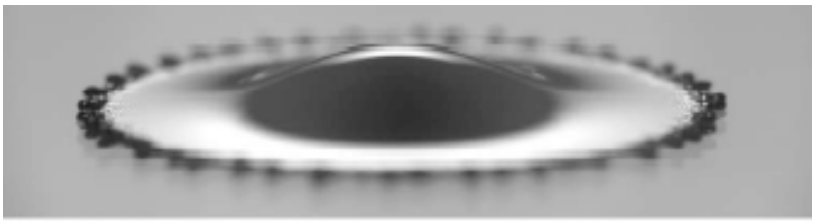

Figure 2.11: Fingering regime adapted from ref. [18].

2.3 Effect of a Crossflow

Injection of a liquid jet in a gaseous crossflow is one of the most efficient spray generation techniques when rapid mixing is desired [22, 23]. Superior mixing properties of this flowfield makes it attractive for power generation and aeronautic propulsion systems, such as low $\mathrm{NO_x}$ gas turbine, High Speed Direct Injection (HSDI) diesel engines, and aircraft engine's afterburner [24, 25]. Among spray characteristics of a liquid jet in a gaseous crossflow, the investigation of droplets' size and velocity distribution is of a great importance as they establish the subsequent features of fuel oxidant mixing quality, such as droplets' spatial distribution, vaporization, mixing rate and consequently the efficiency of liquid fuel combustion [26].

When a droplet is affected by a crossflow, it may deform and be oriented respecting the applied flow. This effect can be attributed to the aerodynamic forces exerted by the gas flow. This flow will also apply additional force to the drop which can vary the outcome of impingement [27]. Furthermore, upon entering the boundary layer at the wall, additional deforming forces are introduced to the droplet which could decelerate and deform the drop slightly before impact [15]. The deformation is caused by an unequal static pressure distribution over the droplet surface, i.e. when a droplet is exposed to a uniform steady gas flow, the velocity of gas has its maximum at the sides of the drop and its minimum at the front and back stagnation points. This, in turn, will cause the droplet to deform from its initial spherical shape into an oblate spheroid, expanding in the radial direction normal to the air flow while decreasing its dimension in the streamwise direction. After reaching the oblate spheroid shape, shear forces and the inner flow inside the droplet cause the side to flatten or even indent, resulting in a spherical cap shape [28]. This deformation can be seen in Figure 2.12.

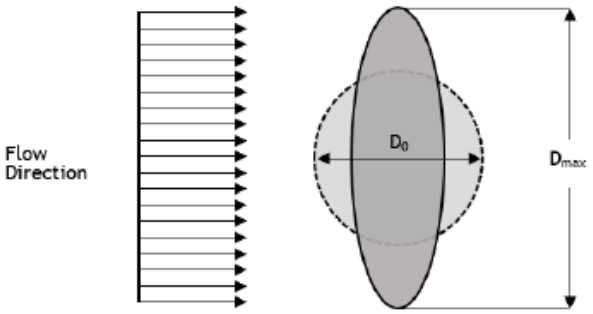

Figure 2.12: Deformation of a droplet due to a crossflow [5, 29, 30].

Several researches were developed in order to understand the effect of the crossflow. The influence on the drop diameter, secondary atomization, velocity of impinging sprays and others are study in ref. [31–34], Figure 2.13. The comparative study between impact with crossflow influence and oblique impact was also preformed previously in order to better understand the droplet deformation influence on impact outcome [35].

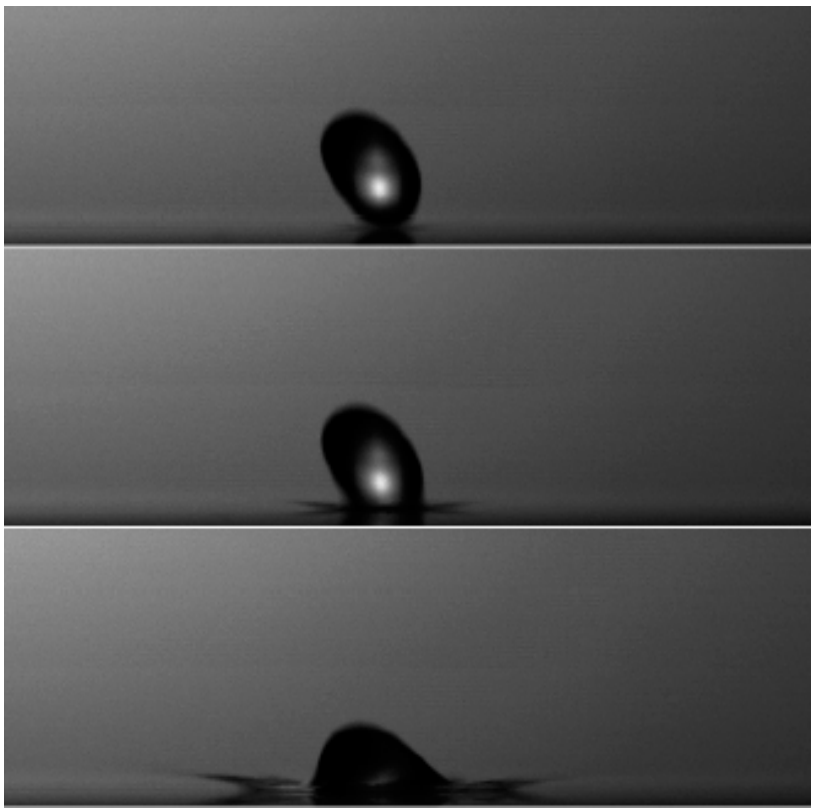

Figure 2.13: Impact with crossflow influence [36].

2.4 Deposition/Splash Transition

The outcome of a droplet impinging on a wall depends on a number of conditions. The phenomena of splash is one of the most required ones and many researchers have focused in the study of this outcome. To properly establish the transition criteria between impingement regimes a

number of empirical correlations have been developed. The criteria presented below only refers to normal impact and/or only considered the normal component of velocity.

Ref. [10] present the splashing parameter ($\mathrm{K_c}$), a correlation which takes the impact velocity and the size of the impacting droplet into consideration on the dynamics of impact, allowing the determination of splash occurrence. It is represented as,

$$K_c = B.Oh^a.We^b \quad (2.8)$$

where a and b depend on experimental conditions. This relation dictates that the transition between the different phenomena occurs when the dimensionless parameters become critical. Ref. [10] includes the effect of the surface roughness with the mean roughness amplitude and observed that rough surfaces exhibit a lower value of $\mathrm{K_c}$, and consequently more splash.

Ref. [17] include the effect of surface roughness by varying the fitting parameters of the correlation, developing criteria for dry and wetted walls depending on the Weber number and surface roughness. For dry surfaces, the transition equation is based on ref. [10] experiment. The boundary limit is represented below,

$$We_c = A.La^{-0.18} \quad (2.9)$$

where the A coefficient depends on the mean surface roughness, Ra. Table 2.2 shows the relation between A and Ra.

Table 2.2: Typical values of the coefficient A depending on the surface roughness adapted from [17].

$Ra\ [\mu m]$	A
0.05	5264
0.14	4534
0.84	2634
3.1	2056
12	1322

Ref. [11] present a model using a combination between the Ohnesorge and Reynolds numbers, not taking in consideration the surface roughness. In this splashing threshold, only the normal impact velocity is considered. For the impact surface used to produce the data, two discs were considered, one with smooth surface and the other with rough surface.

$$K_c = Oh.Re^{1.25} = 57.7 \quad (2.10)$$

Their experiment shows that deposition transitions to splash when $K_c = 57.7$, meaning that, above this value splash occurs and below deposition is observed.

Ref. [37] developed the last criteria used in this dissertation. For the development of their study to determine the empirical correlation for the non-splash/splash boundary. it was considered

an aluminium disk with a surface roughness of $0.01\,\mu\mathrm{m}$.

$$K_c = Oh.Re^{0.609} = 0.85 \quad (2.11)$$

This correlation fits well for high Reynolds numbers. However, when viscous forces and wettability effects become more significant does not fit well.

Chapter 3

Experimental Setup

This chapter is focused on the experimental setup. Firstly, the experimental facility is introduced with a brief description of the characteristics of the most important components. Secondly, the methodology is presented in order to understand the process used to obtain the experimental results in this dissertation. The physical properties that govern the dynamic behaviour of a impacting droplet is outlined and described in the fourth section. Finally, a description of the image data processing and analysis is presented.

3.1 Experimental Facility

To achieve the necessary conditions for the present work an experimental facility is used, previously designed by refs. [36, 38]. The experimental arrangement is composed of an impact surface, a wind tunnel, a system for image acquisition, a droplet dispensing system and a LED illumination set. During the experiments, the temperature of the air and humidity of the laboratory were kept constant (temperature at $22° \pm 1°$ and humidity at 50%).

The droplets are generated by a droplet dispensing system that is composed of a syringe pump, and a needle attached with the help of a circular tube. A computer is also used to control this system which releases the fluid with a specific pumping rate. A structure is used to support all of the components and will enable the needle height variation. This structure is visible in Figure 3.1.

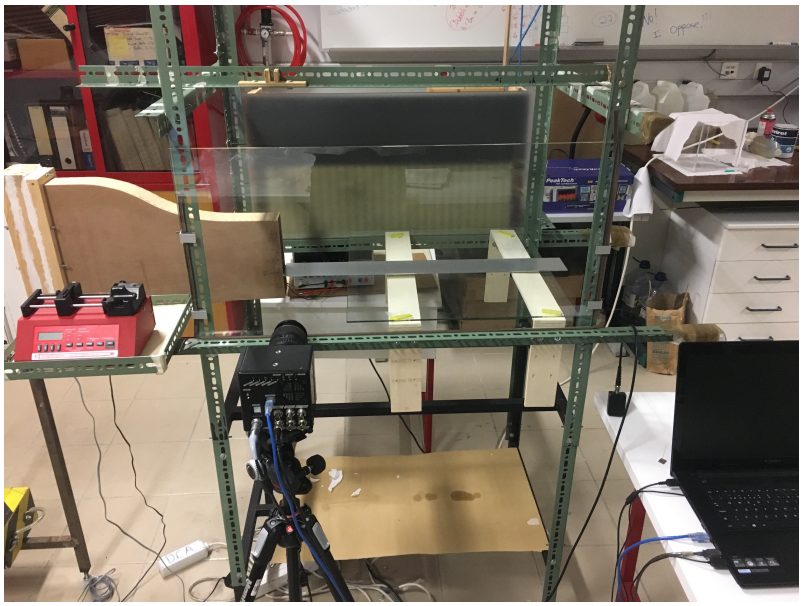

Figure 3.1: Experimental facility.

3.1.1 Wind tunnel

To study the droplet impact onto a surface with the influence of a crossflow, the knowledge and use of a wind tunnel is indispensable. This wind tunnel is constituted of a diffuser, a setting chamber and a contraction. The diffuser is used to decelerate the flow and was designed with the following specifications: $335\,\mathrm{mm}$ of length and an angle of $48.24°$.

According to [39], the setting chamber consists of honeycomb and screens as seen in Figure 3.2. The honeycombs are effective to remove swirl and lateral mean velocity variations, providing that the flow yaw angles are lower than $10°$. The screen allows a more uniform velocity profile of the flow and reduces the boundary layer thickness, giving the flow an increased ability to withstand a pressure gradient.

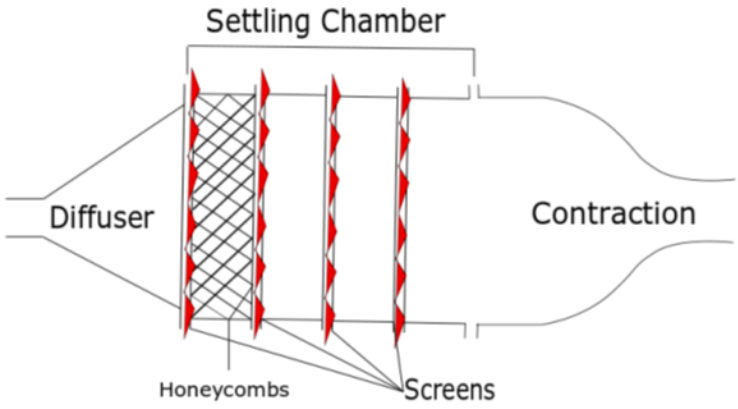

Figure 3.2: Wind tunnel schematics with element placement [36].

The spacing of the screens must be enough for static pressure to fully recover from a perturbation before reaching the next one, and minimum spacing should be the magnitude of the eddy containing the maximum energy. Contrary to the diffuser, the contraction is used to accelerate the flow, allowing the placement of the screens and honeycombs in a low-speed area to reduce pressure losses. The length of the contraction is important because, if it is big enough, it will avoid separation but, consequently, will increase the boundary layer thickness. Designed by ref. [40], the exit nozzle has $200 \times 40\,\mathrm{mm}$, Figure 3.3.

Figure 3.3: Nozzle exit of the contraction developed by ref. [40].

3.1.2 Droplet Dispensing System

The droplet generation is done using a NE-1000 Single Syringe Pump, Figure 3.4. This system has a range of $1.459\,\mu\mathrm{l/h}$, for a $1\,\mathrm{mL}$ syringe, to $127.2\,\mathrm{ml\,min^{-1}}$ for a $60\,\mathrm{mL}$ syringe. In this study, $50\,\mathrm{mL}$ syringes with a pumping rate of $0.5\,\mathrm{mL\,min^{-1}}$ are used.

The droplet is originated at the tip of the needle and detaches when gravity exceeds the surface tension forces, allowing a drop generation with a negligible initial velocity. The pump rate is remotely operated by a computer software, making it more efficient and practical.

Figure 3.4: Syringe pump.

A stainless steel needle is attached to the syringe through an appropriate tube so the pump can be in a static stable mount, reducing unwanted vibrations. The needle has an inner diameter of $\mathrm{D_{in}} = 1.50\,\mathrm{mm}$. To avoid contamination, different needles are used for each fluid, Figure 3.5.

Figure 3.5: Stainless steel needles.

3.1.3 Image Acquisition System

The camera used in this dissertation, as shown in Figure 3.6, is a Photron FASTCAM mini UX50, with $1.3\,\mathrm{megapixel}$ image resolution at frame rates from $2000\,\mathrm{fps}$ up to $160\,000\,\mathrm{fps}$ at reduced image resolution. This is a high-speed digital camera that allows us to acquire images with an acceptable accuracy and quality. A Macro Lens Tokina AT-X M100 AF PRO D was attached to the camera with a minimum focus distance of $300\,\mathrm{mm}$, a focal length of $100\,\mathrm{mm}$, a 1:1 macro ratio and a filter size of $55\,\mathrm{mm}$.

Figure 3.6: High-speed camera.

For the present study, the characteristics of image capture are altered using the camera's computer software. The frame rate was set at $4000\,\mathrm{fps}$, $8000\,\mathrm{fps}$ and $10\,000\,\mathrm{fps}$, corresponding to a resolution of $1280\mathrm{x}512$, $296\mathrm{x}1280$ and $240\mathrm{x}1280$ respectively. The shutter (exposure time) is set at $1/20\,000\,\mathrm{s}$, $1/25\,000\,\mathrm{s}$ and $1/25\,600\,\mathrm{s}$.

3.1.4 Illumination System

For a clear visualization of the phenomena, there is a need of providing a good illumination system. In the experiments it is used a 96W LED ribbon attached to a wooden panel connected to a power supply. This converts alternated into direct current eliminating the light flickering, obtaining a more efficient and uniform illumination, Figure 3.7. To improve the visualization of the images, the room is kept completely dark with only the LED switched on during the image acquisition. For a uniform illumination, a diffusion glass was placed between the LED lighting and the impact surface. It is important to mention that this illumination is parallel to the droplet trajectory plane.

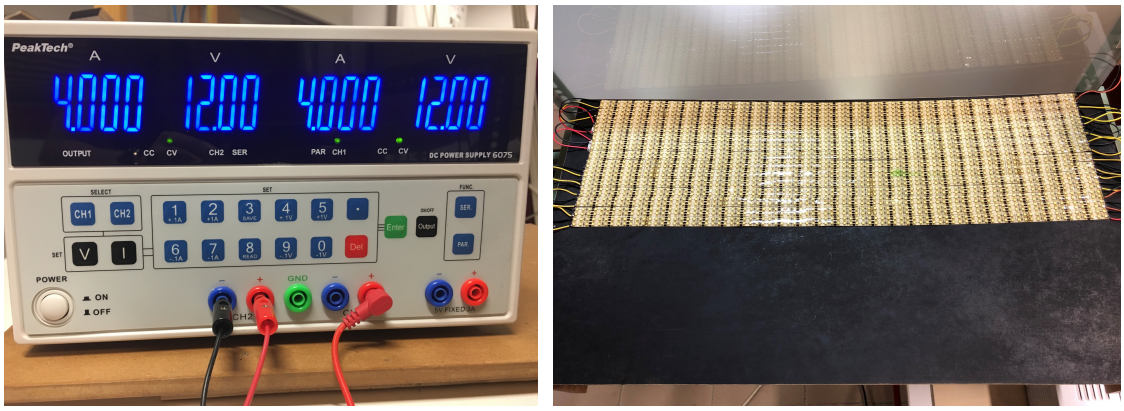

(a) (b)

Figure 3.7: Illumination set: a) Power supply, b) LED panel.

3.1.5 Impact Surface

Several factors constrain the single droplet impingement, one of them being the impact surface and its characteristics. As described in [36], the surface is a smooth aluminium plate with $700\text{x}80\text{mm}$, as seen in the Figure 3.8.

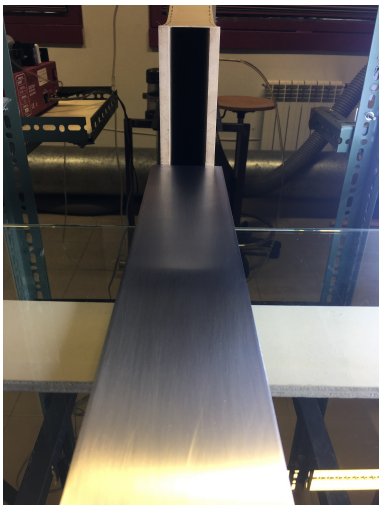

Figure 3.8: Aluminium impact surface.

While performing the tests with the crossflow, the aluminium plate is placed across the exit nozzle and equidistant to the two glasses. The plate is placed 70mm above the lower boundary of the exit nozzle to enable a stable crossflow.

Knowing the importance of surface roughness for the development of the phenomena, a measure of the plate roughness is made using a roughness tester, more concretely a Hommel Tester T1000. Three tests were performed analysing a $4.8\,\text{mm}$ length section. Ref. [36] impact surface presents a surface roughness of $0.19\,\mu\text{m}$ previously measured by ref. [5].

Is important to mention that, between tests, the surface is thoroughly cleaned in order to maintain the properties and not condition results.

3.2 Methodology

When performing any measurement or experimental test, a detailed plan of the methodology is required in order to minimize waste of fuel and errors. This section is devoted to the methodology followed in this work. The present work presents two different phases.

The first phase is related to the study of normal impact and impact with a crossflow velocity of $7\,\mathrm{m\,s^{-1}}$. This phase begins ensuring that the high-speed camera is kept parallel to the droplets trajectory following the definition of a needle hight and the observation of the resulting phenomenon and the determination of the impact velocity. Finally the injection needle is then varied in order to found the transition between non-splash and splash.

The second phase refers to the crossflow velocity variation study and starts with the calibration of the wind tunnel so to ensure the correct flow velocity. Once the confirmation is made for the occurrence of splash and respective impact velocity for a crossflow velocity of $7\,\mathrm{m\,s^{-1}}$ the last is gradually increased in a way to verify its influence on droplet impact outcome. It is important to mention that in this last phase only the crossflow velocity is varied and not the injection needle hight.

3.3 Fluid Properties

In this dissertation, four fluids were considered: $100\,\%$ JF, $75\,\%$ JF - $25\,\%$ HVO, $50\,\%$ JF - $50\,\%$ HVO and H_2O, where HVO is the NEXBTL Hidro-processed Vegetable Oil and the jet fuel is Jet A-1. The use of water is important because it is a reference fluid and its properties are well reported in the literature. However, the main fluid properties ($100\,\%$ JF and mixtures) are not well established and must be measured before the experiments. The main properties (density, surface tension and viscosity) are presented.

As the current legislation allows a maximum of $50\,\%$ in volume for alternative fuels, only the mixtures stated above are considered [2].

Properties

Density, ρ, is defined as the ratio between mass and volume of an homogeneous solution at a specific temperature [41]. Being, in equation form,

$$\rho = \frac{m}{V} \quad (3.1)$$

where m, [kg], is the mass and V, [$\mathrm{m^3}$], the volume of the substance to be measured.

Surface tension, σ, is given by the specific energy of liquid surface at the interface of another fluid. Regularly, values for surface tension are given when the surface of the liquid is in contact with the air [41].

The viscosity, μ, is defined as a measure of the fluids internal resistance to motion caused by cohesive forces among the fluid molecules [41].

The values for the fluid physical properties used in this experimental work are listed in the Table 3.1.

Table 3.1: Fluid properties adapted from [36].

	$100\,\%$JF	$75\,\%$JF-$25\,\%$HVO	$50\,\%$JF-$50\,\%$HVO	H_2O
$\rho\ [kg/m^3]$	798	795	792	1000
$\sigma\ [mN/m]$	25.4	25.5	24.6	72.0
$\mu\ [mPa.s]$	1.12	1.44	1.79	1.0

As it can be seen, the density is higher for the water and lower for $100\,\%$JF, decreasing in the mixtures with the increase of HVO percentage. Regarding the surface tension, the value for $100\,\%$JF and mixtures are similar but triples in value for the water. In terms of viscosity, $100\,\%$JF and water present similar values and, for the mixtures, the value increases with HVO percentage increase.

3.4 Image Data Processing

To study this phenomena it is crucial the knowledge of droplet diameters, impact velocities, and dimensionless numbers. Therefore, image data processing is used to acquire this information with the aid of ®MATLAB software, using [5] algorithm adapted from the work of [38]. The adopted methodology is specified in this section.

3.4.1 Pixel Sizing

All the data is recovered in pixels since all the experimental footage is retrieved through a high-speed digital camera. The measure of the pixel is made using a reference, Figure 3.9. This sizing is made using a correspondence between the number of pixels in the image and the size of the reference in millimetres. In this work, two references are used, two needles with a exterior diameter of $\mathrm{D_{out}} = 1.27\,\mathrm{mm}$ and $\mathrm{D_{out}} = 0.79\,\mathrm{mm}$.

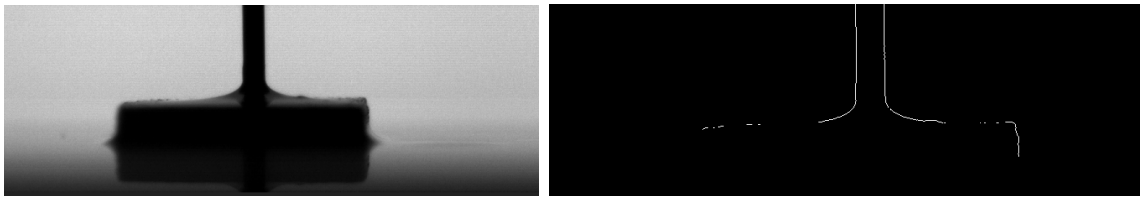

(a) (b)

Figure 3.9: Reference: a) Snapshot acquired using the camera's software, b) Reference snapshot in binary outlining the contour.

With the aid of a Matlab®algorithm, the image is read by an "$inhouse$" built code that outlines the needles out contours and measures the number of pixels. Considering approximately fifteen lines of the image, the algorithm counts the number of pixels existent between the boundaries of the needle.

According to ref. [41], the measurements of a length in digital image with grey values associated with the pixel positions can only be determined with an accuracy of $\pm 0.5\mathrm{pixel}$.

3.4.2 Droplet Diameter

Previously determined in the work of [38], the diameters of the droplets used in this dissertation are presented in the Table 3.2.

Table 3.2: Droplet diameters.

	100 %JF	75 %JF-25 %HVO	50 %JF-50 %HVO	H_2O
$D\ [mm]$	3.0	3.1	3.1	4.1

3.4.3 Impact Velocity Determination

The impact velocity of a droplet is crucial for the determination of the dimensionless numbers. For this, three images are considered, the background, the image of the droplet in the moment before impact and one 7 frames before impact, Figure 3.10. This allows the determination of the position of the droplet centroid, making possible an approximation of the general trajectory of the droplet.

The images are retrieved at $4000\,\mathrm{fps}$, $8000\,\mathrm{fps}$ and $10\,000\,\mathrm{fps}$, meaning a time-step of $1.75\mathrm{ms}$, $0.875\mathrm{ms}$ and $0.7\mathrm{ms}$, respectively. Knowing the time and distance travelled between images, the velocity is calculated.

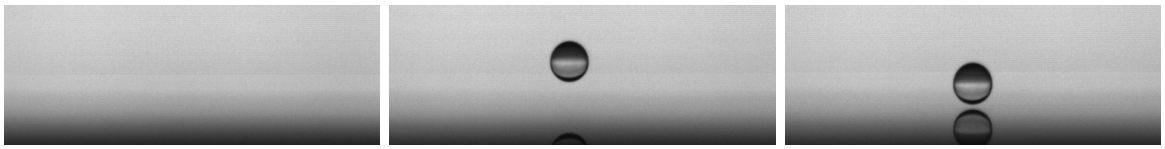

(a) (b) (c)

Figure 3.10: Images for impact velocity : a) Background image, b) Droplet image 7 frames before impact, c) Droplet image prior to impact.

For the first phase two frame rates were used. For the same impact condition it was verified that the impact velocity was $1.69\,\mathrm{m\,s^{-1}}$ and $1.71\,\mathrm{m\,s^{-1}}$ for $4000\,\mathrm{fps}$ and $8000\,\mathrm{fps}$ respectively, presenting a difference of $0.02\,\mathrm{m\,s^{-1}}$. For the second phase it was used the $8000\,\mathrm{fps}$ and $10\,000\,\mathrm{fps}$ frame rates and it was verified a impact velocity of $2.3\,\mathrm{m\,s^{-1}}$ and $2.28\,\mathrm{m\,s^{-1}}$ respectively.

Chapter 4

Results and Discussion

This chapter details the results obtained in the experimental study and is divided in three sections: phenomena visualization, splash threshold and summary, where the results are presented and discussed.

Firstly, the visualization and development of each regime for normal impact and impact under the influence of crossflow are listed. The study of the variation crossflow velocities is, then, presented in order to understand the influence of each velocity component (normal and tangential) on the phenomena outcome.

Secondly, the threshold is presented for normal impact and crossflow impact. Following the comparison of the experimental results with empirical correlations developed by other researchers. Finally, the most important conclusions are briefly presented in a summary

4.1 Phenomena Visualization

The following section is divided in three subsections: normal impact, impact under the influence of crossflow velocity of $7\,\mathrm{m\,s^{-1}}$ and crossflow velocity variation study.

In the case of the drop impact on a surface, two stages can be recognized. Firstly, after coming into contact with the surface, the drop moves vertically down and the liquid is being radially spread over the surface until it reaches the maximum diameter. Secondly, after the lamella reaches its maximum spreading, the lamella contact line either recedes or sticks to the surface [42].

4.1.1 Normal Impact

In this experimental work, three regimes are found for normal impact: deposition, fingering and prompt splash. The results are presented based on the impact energy necessary to produce such phenomena. A normal impact refers to a droplet impingement perpendicular to a stationary surface as represented in Figure 4.1.

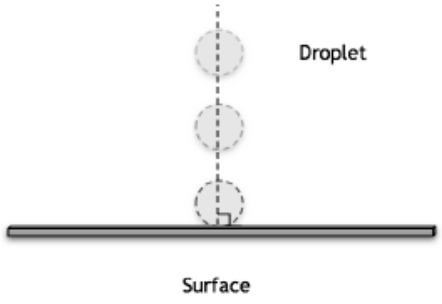

Figure 4.1: Normal impact adapted from [5].

In Figure 4.2, there is a sequence of images which shows deposition for the 50% JF - 50% HVO mixture. This occurs when the droplet impacts on a surface with moderate velocity and spreads out to form a film wall. Before impact the droplet is spherical, as seen in the instant $\tau = -0.07$. The impact moment corresponds to $\tau = 0$ and in the following frame, which corresponds to $\tau = 0.07$, splash is not observed, i.e., no secondary atomization occurred. After impingement the lamella starts to spread evenly on both sides. When reaching the maximum spread diameter it recoils and sticks to the wall.

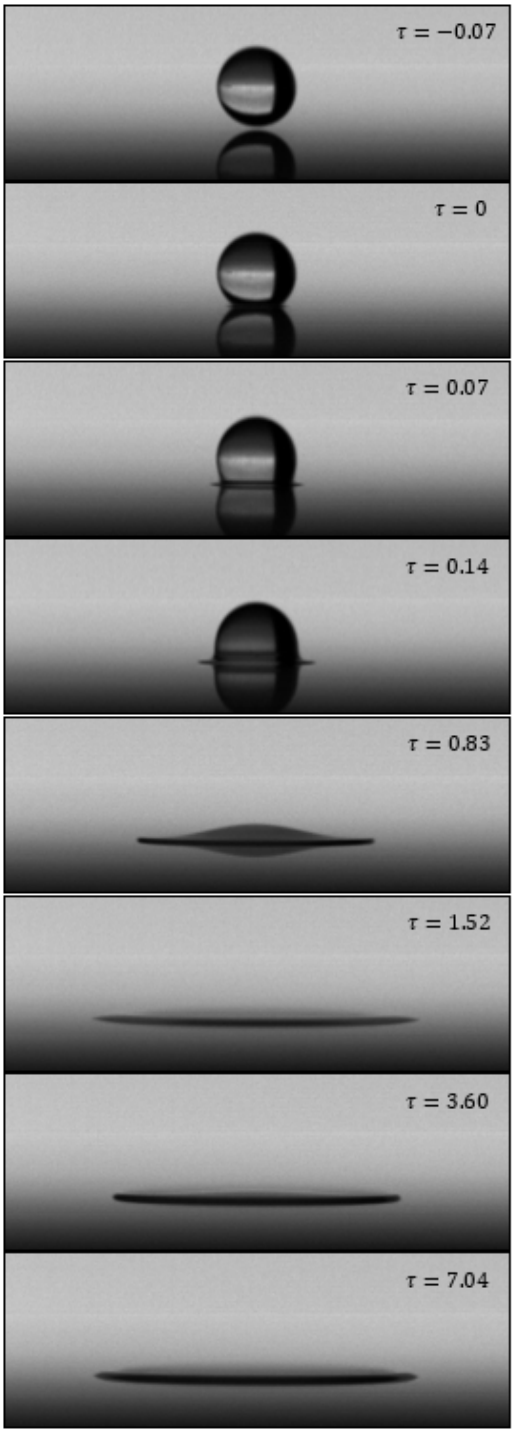

Figure 4.2: Spreading for 50% JF - 50% HVO mixture ($\mathrm{D_0} = 3.1\mathrm{mm}$, $\mathrm{U} = 1.7\mathrm{m.s^{-1}}$).

In Figure 4.3, the fingering phenomena is presented for H_2O. Fingering appears when the outer rim of the lamella suffers disturbances during the spreading phase creating finger-like shapes. Similar to the spread regime, before impact the droplet is spherical. Following the moment of impact, no secondary atomization occurs, $\tau = 0.07$, and the lamella starts to spread radially allowing the initial visualization of fingering, $\tau = 1.50$. When reaching the maximum spread diameter, one is able to observe the finger structures' complete formation ($\tau = 3.55$), later originating receding and stick events.

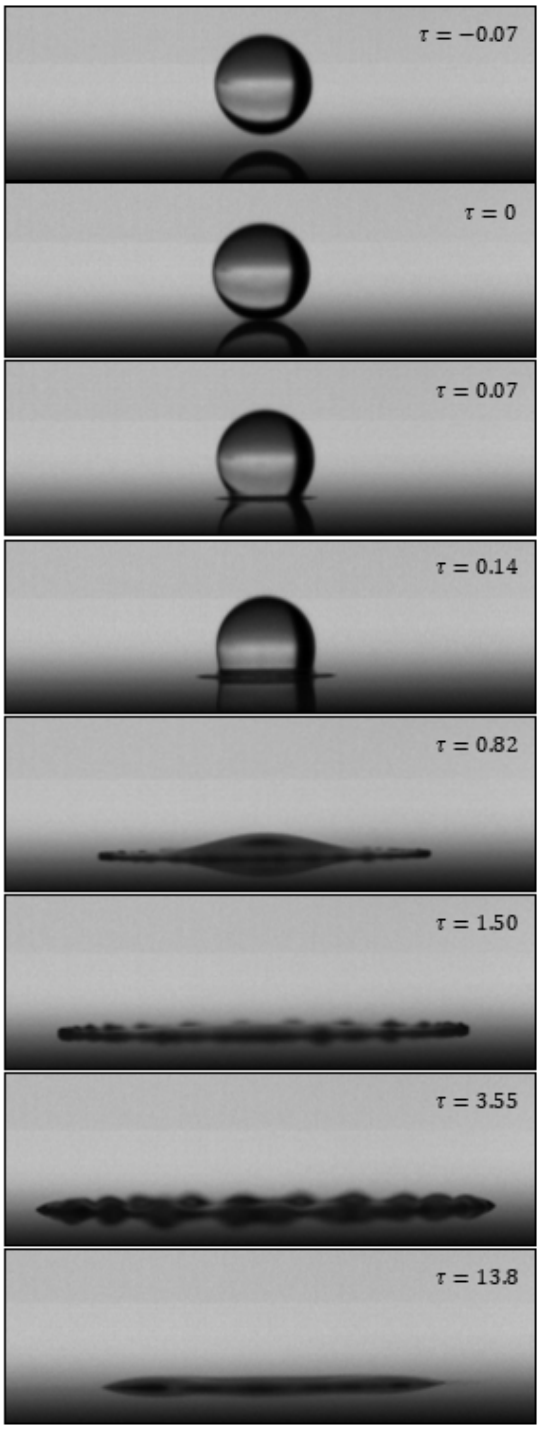

Figure 4.3: Fingering phenomena for H_2O ($D_0 = 4.1\text{mm}$, $U = 2.2\text{m.s}^{-1}$).

Prompt splash regime for 75% JF - 25% HVO droplet is displayed in Figure 4.4. Splash occurs for high Reynolds numbers and is characterized by the formation of smaller droplets on the periphery of the rim. Similar to the previous case, the droplet is spherical before impact. After the impingement ($\tau = 0$) prompt splash occurs at upstream and downstream, $\tau = 0.09$. On both instants, it is possible to observe the secondary droplets being ejected from the rim while the spreading phase is maintained.

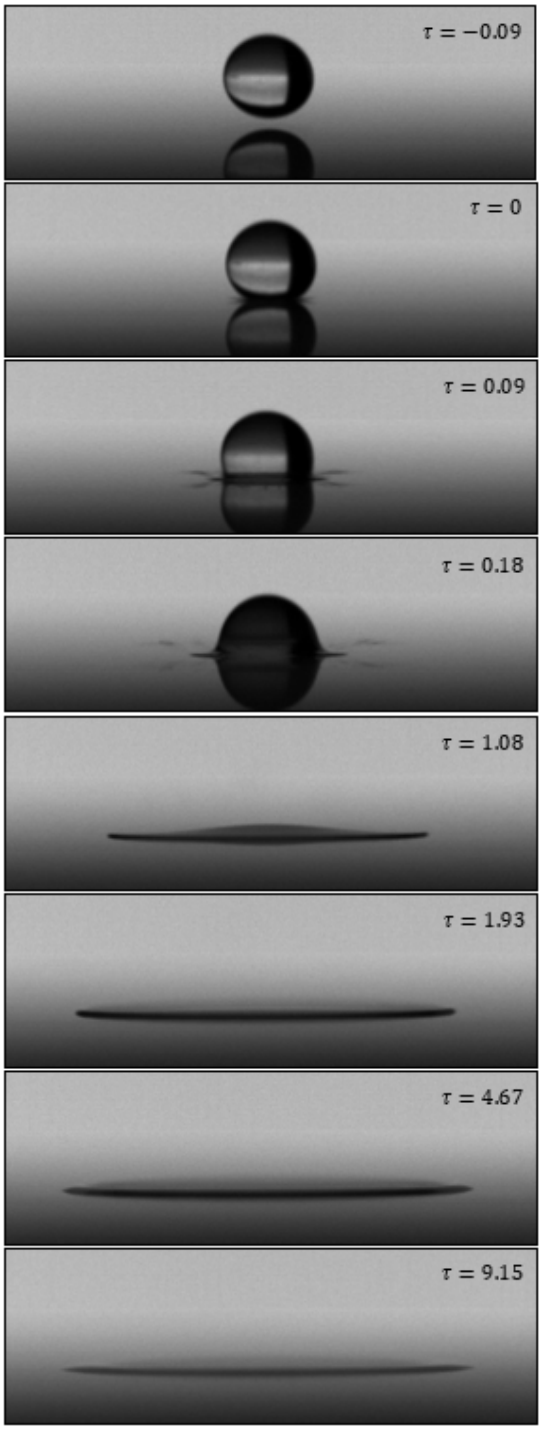

Figure 4.4: Prompt splash regime for 75% JF - 25% HVO ($\mathrm{D_0} = 3.1\mathrm{mm}$, $\mathrm{U} = 2.2\mathrm{m.s^{-1}}$).

4.1.2 Impact with Crossflow

All the tests considered for the study present in this section were performed with a crossflow velocity of $\mathrm{U_{cf}} = 7\,\mathrm{ms^{-1}}$ and a left to right flow direction. The droplet suffers a certain deformation due to the influence of crossflow which conditions the impact, that translates into an impingement where the droplet will impact with normal and tangential impact velocity. This will create a certain angle defined as the incident angle (θ). The incident angle represents the angle between the absolute impact velocity and the surface. Figure 4.5 displays a representation of the droplet behaviour under the influence of the crossflow and the orientation of the fluid flow. Figure 4.6a displays the deformation upon impact and Figure 4.6b represents the azimuthal direction on a impinging droplet.

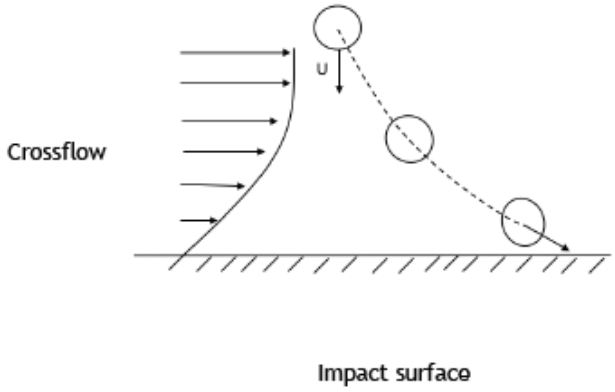

Figure 4.5: Droplet impingement behaviour under the influence of a crossflow and fluid flow orientation adapted from [5].

(a) (b)

Figure 4.6: Impact: a) deformation on impact and b) azimuthal direction.

A droplet of 50% JF - 50% HVO impinging in a smooth dry wall under the influence of crossflow is displayed in Figure 4.7 representing the spread phenomena. Spreading of a drop on a surface influenced by a crossflow is due to two facts: first, drop's initial kinetic energy; second, momentum transfer from the surface to the lamella. The former leads to lamella expansion around the liquid body of the drop and the latter stretches the lamella in the direction of the flow.

Before impact the droplet is deformed due to the crossflow. After the impact, the droplet spreads without secondary atomization creating a film wall. When the maximum spread ratio is attained the film wall starts to slide in the flow direction.

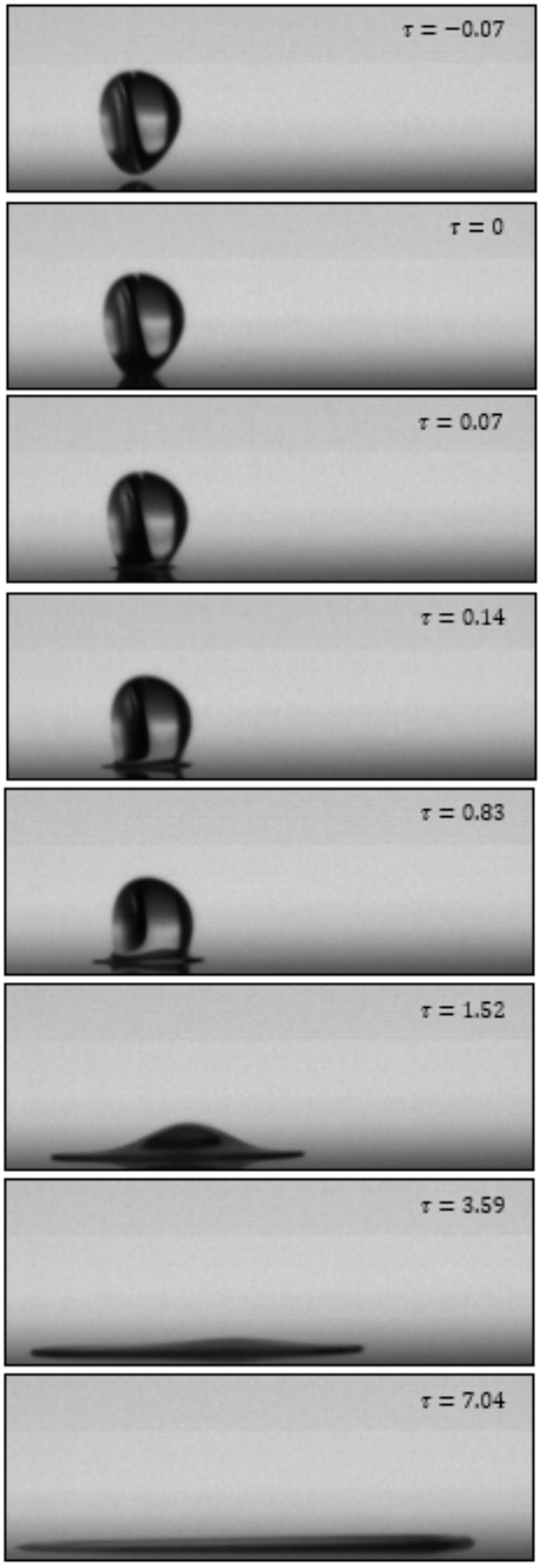

Figure 4.7: Spread regime development with crossflow effect for 50% JF - 50% HVO droplet ($\mathrm{D_0} = 3.1\mathrm{mm}$, $\mathrm{U} = 1.7\mathrm{m.s^{-1}}$).

Figure 4.8 presents the development of fingering for a $\mathrm{H_2O}$ droplet impinging with crossflow effect. For the same crossflow velocity, due to its' greater surface tension, an $\mathrm{H_2O}$ drop does not suffer much deformation when compared to the other test fluids. Impinging on the surface

at $\tau = 0$ the droplet spreads and starts to develop fingering in the outer rim ($\tau = 0.46$). Similar to the case mentioned above, once the maximum spread ratio is reached ($\tau = 2.44$), the fluid slides in the direction of the flow.

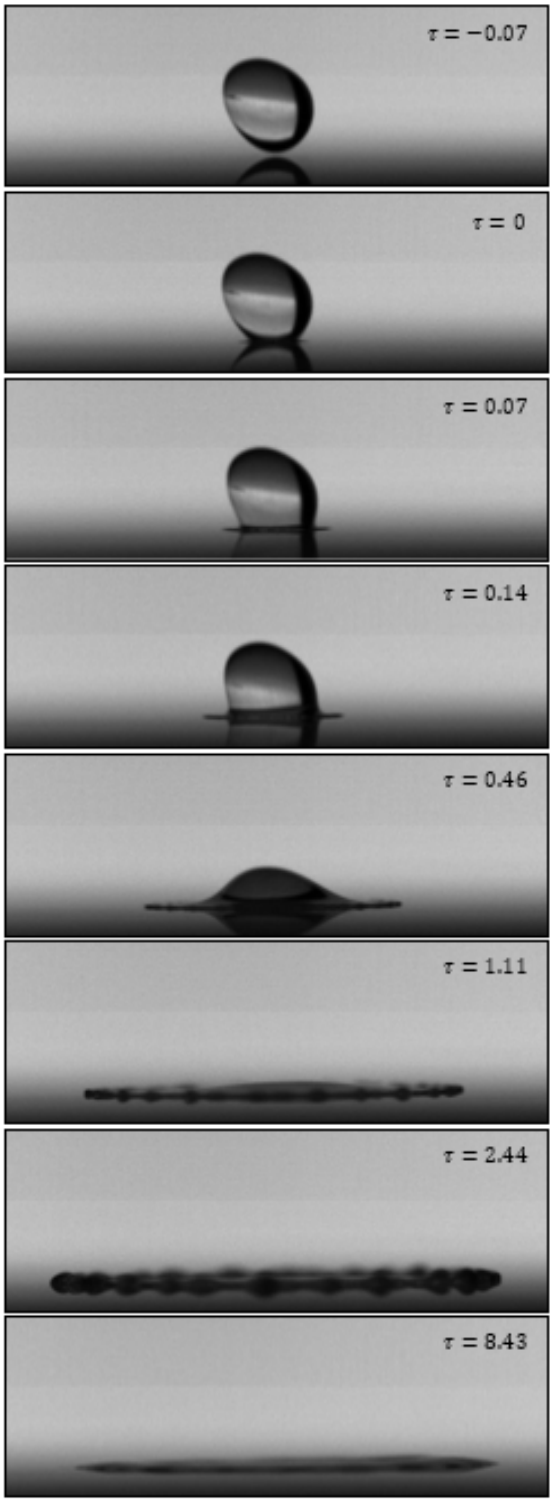

Figure 4.8: Fingering regime development with crossflow effect for $\mathrm{H_2O}$ droplet ($\mathrm{D_0} = 4.1\mathrm{mm}$, $\mathrm{U} = 2.7\mathrm{m.s^{-1}}$).

Figure 4.9 displays the prompt splash regime for an 100% JF droplet. As can be observed the droplet is deformed before impact ($\tau = -0.07$). In instant $\tau = 0.09$, it is possible to notice that

prompt splash occurs on the left side of the droplet. One is able to perceive that the ocurrence of splash is greater on the left side than on the right side ($\tau = 0.19$), this phenomenon will be presented in the following section. As the lamella spreads, it is possible to observe the development of the splash as the secondary droplets are ejected from the outer rim of the lamella. When reaching the maximum spread ratio ($\tau = 2.20$), it slides in the direction of the flow.

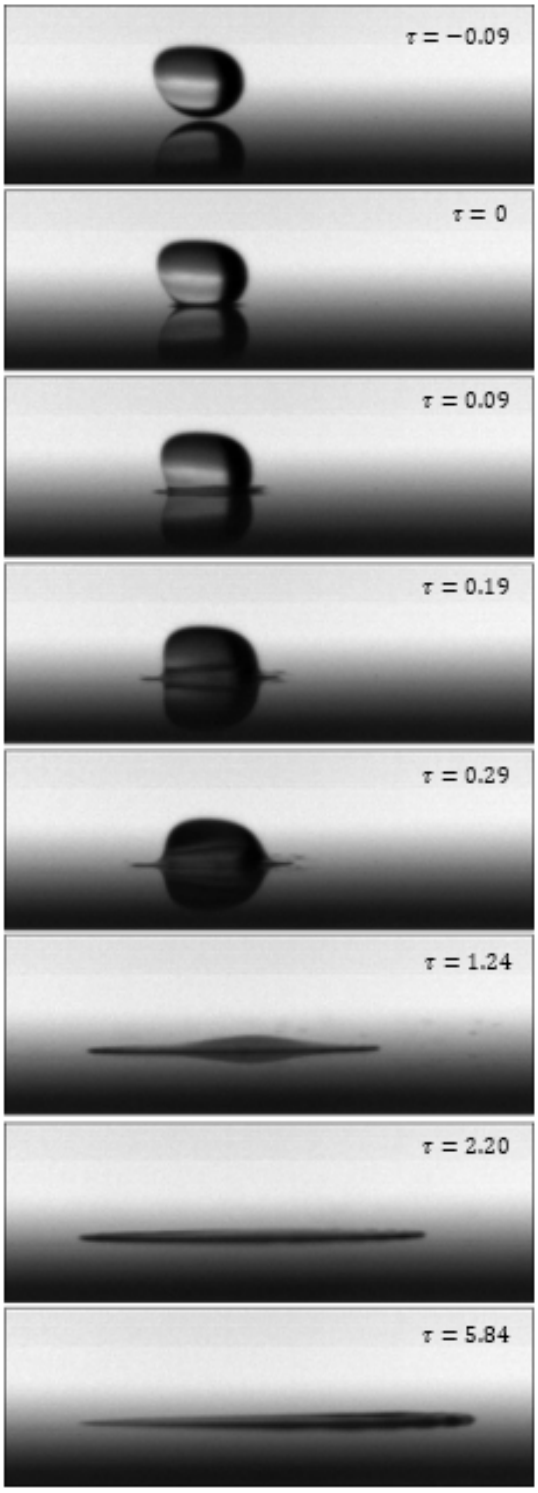

Figure 4.9: Prompt splash regime development with crossflow effect for 100% JF droplet ($\mathrm{D_0} = 3.0\mathrm{mm}$, $\mathrm{U} = 2.3\mathrm{m.s^{-1}}$).

The development of the corona splash regime for a 75% JF - 25% HVO droplet is displayed in Figure 4.10. Before impact the droplet is slightly deformed. At the moment of impact ($\tau = 0$) is possible to notice secondary atomization. Crown starts to rise, and tinny droplets are ejected in the periphery ($\tau = 0.12$), when the lamella reaches a certain thickness, the crown is ruptured ($\tau = 0.23$), and secondary droplets are ejected as the lamella spreads ($\tau = 1.39$).

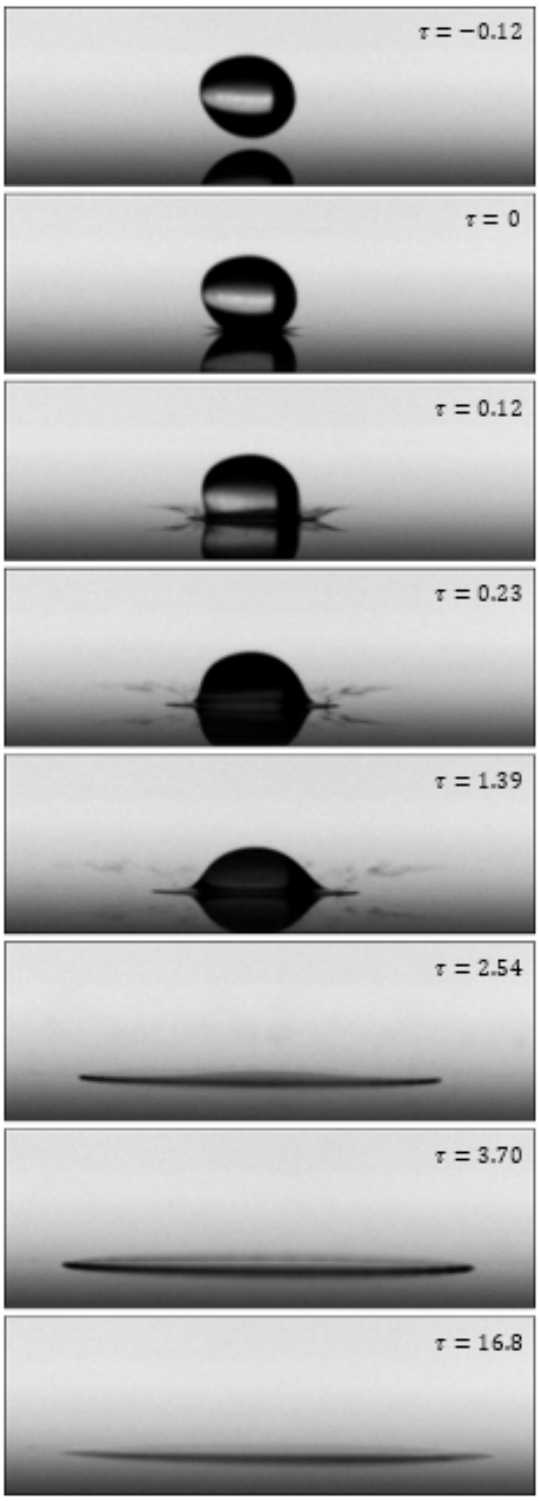

Figure 4.10: Corona splash regime development with crossflow effect for 75% JF - 25% HVO droplet ($\mathrm{D_0} = 3.1\mathrm{mm}$, $\mathrm{U} = 2.8\mathrm{m.s^{-1}}$).

4.1.3 Crossflow Variation Study

All the tests considered for the study presented in this section were performed with a crossflow velocity, U_{cf}, of $7\,m\,s^{-1}$, $10\,m\,s^{-1}$, $12\,m\,s^{-1}$ and $15\,m\,s^{-1}$, and a left to right flow direction. For this study, the normal velocity of impingement was kept constant for each fluid, being this velocity, the one where splash first occurred for $U_{cf} = 7 m.s^{-1}$ and only the crossflow velocity was increased.

4.1.3.1 H_2O (water) impingement

Figure 4.11 displays the impingement for a H_2O droplet with an influencing crossflow of a) $7 m.s^{-1}$, b)$10 m.s^{-1}$ and c) $15 m.s^{-1}$.

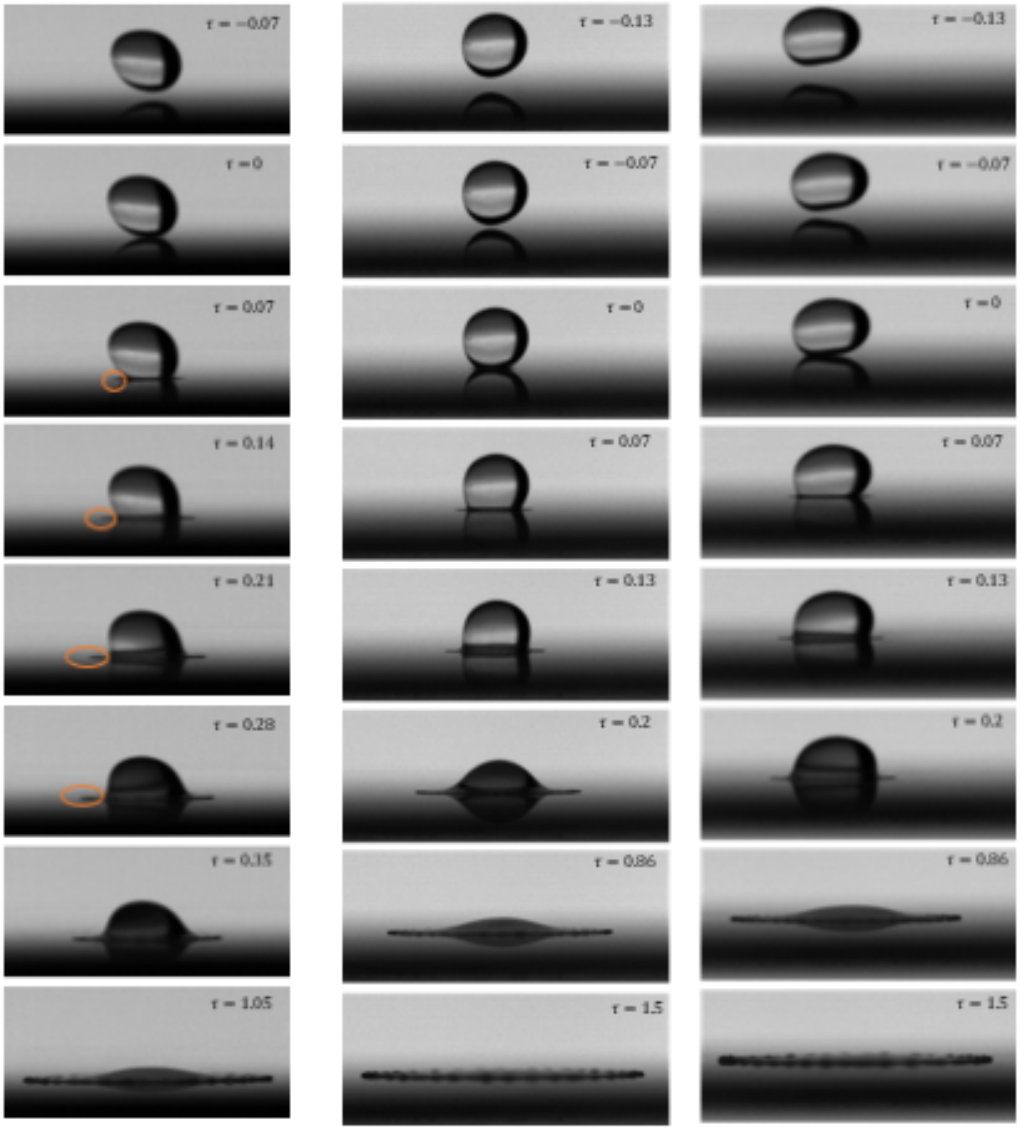

(a) (b) (c)

Figure 4.11: H_2O droplet impingement with a crossflow velocity of: a) $7\,m\,s^{-1}$, b) $10\,m\,s^{-1}$, c) $15\,m\,s^{-1}$.

One is able to perceive that the initial deformation is different for each velocity, having for the first two velocities an elongated deformation and for the last a transversal deformation

creating a bean-like shape. This may occur due to the fact that this last velocity is near the breakup regime velocity. In Figure 4.11a, at $\tau = 0.07$, is possible to observe prompt splash on the left side (upstream). Here, tiny droplets are generated at the contact line of the lamella while it spreads. However, when the crossflow velocity is increased, Figure 4.11b, the small droplets are smoothed by the flow and no secondary atomization occurs ($\tau = 0.07$), the lamella spreads asymmetrically and fingering is observed. The droplet, displayed in Figure 4.11c, having a transversal deformation, when it impacts the surface prompt splash occurs on the right side (downstream), $\tau = 0.07$. The small droplets move upward and on the direction of the flow.

4.1.3.2 100% JF impingement

Figure 4.12 displays the impingement for a 100% JF droplet with an influencing crossflow of a) $7\mathrm{m.s}^{-1}$ and b)$10\mathrm{m.s}^{-1}$.

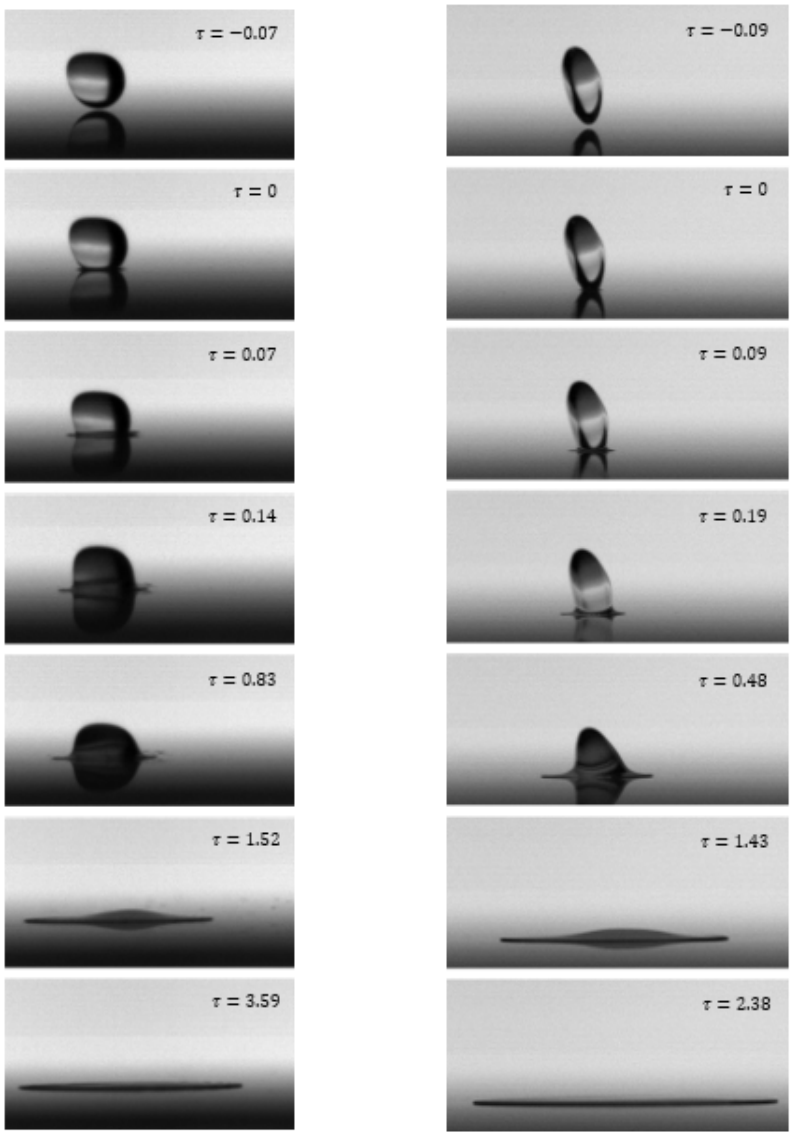

(a) (b)

Figure 4.12: 100% JF droplet impingement with a crossflow velocity of: a) $7\,\mathrm{m\,s}^{-1}$ and b) $10\,\mathrm{m\,s}^{-1}$.

Similar to the case stated before, in Figure 4.12a is displayed the development of impingement of a droplet of 100% JF. Here, after the moment of impact, it is possible to notice the development of prompt splash downstream, $\tau = 0.07$. These tiny droplets build up while the lamella spreads, moving in the direction of the flow, $\tau = 1.52$. Figure 4.12b displays the development of a droplet of the same fluid but influenced by $\mathrm{U_{cf}} = 10\mathrm{m.s^{-1}}$. Due to the shear forces and internal flow of the droplet, this droplet is deformed in a way that the side is flatten resulting in a cap shape geometry. The increasing of crossflow velocity works in way that smooths the small droplets presented on the case before and no secondary atomization is observed, $\tau = 0.09$.

4.1.3.3 75% JF - 25% HVO impingement

Figure 4.13 displays the impingement for a 75% JF - 25% HVO droplet with an influencing crossflow of a) $7\mathrm{m.s^{-1}}$ and b) $10\mathrm{m.s^{-1}}$.

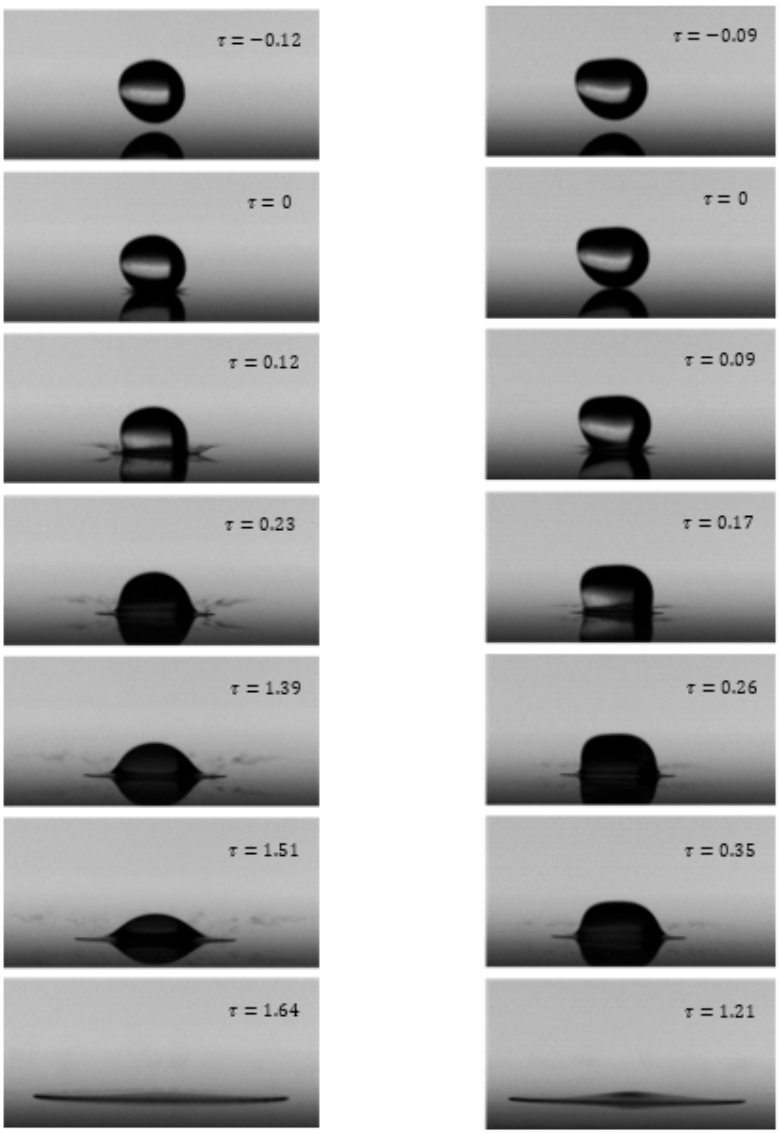

(a) (b)

Figure 4.13: 75% JF - 25% HVO droplet impingement with a crossflow velocity of: a) $7\,\mathrm{m\,s^{-1}}$ and b) $10\,\mathrm{m\,s^{-1}}$.

The development of a 75% JF - 25% HVO droplet impinging on a surface with the influence of a crossflow with $\mathrm{U_{cf}} = 7\mathrm{m.s^{-1}}$ is displayed in Figure 4.13a. As already stated in section 4.1.2, when the drop impacts the surface, asymmetric corona splash occurs, $\tau = 0.12$. The lamella lifts off around the drop contact line in an azimuthally asymmetric form, i.e., it gradually decreases in the azimuthal direction along the lamella contact line from points $\varphi = 0°$ to $\varphi = 180°$.

Figure 4.13b displays the development of the droplet influenced by a crossflow of $\mathrm{U_{cf}} = 10\mathrm{m.s^{-1}}$. The increasing of tangential velocity smooths the secondary droplets upstream and prompt-corona splash occurs, $\tau = 0.17$, i.e., detachment of tiny droplets from the advancing contact line at upstream and corona splashing at downstream.

A crossflow velocity of $\mathrm{U_{cf}} = 12m.s^{-1}$ was also tested for this fuel mixture. However, due to the proximity of this velocity to the breakup regime, two outcomes are observed, Figure 4.14.

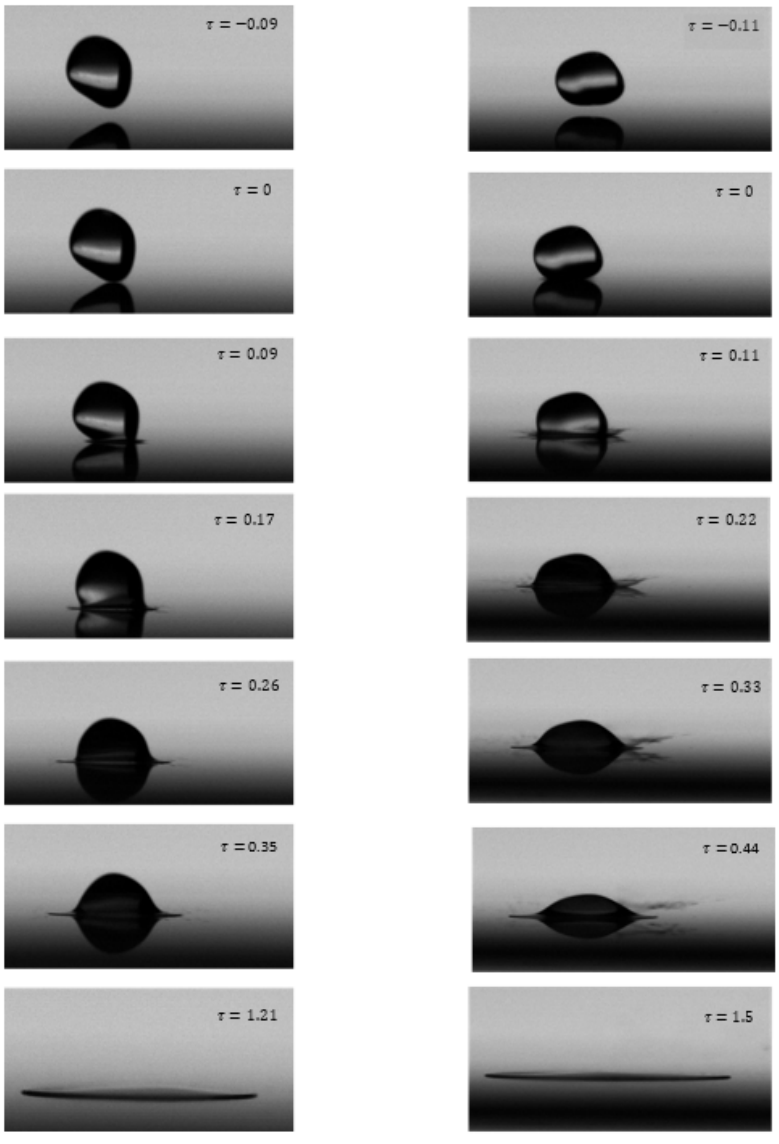

Figure 4.14: Outcomes of 75% JF - 25% HVO droplet impingement with a crossflow velocity of $12\,\mathrm{m\,s^{-1}}$.

One is able to notice that the droplet deformation has a great influence on the impact outcome.

Two deformation shapes were observed: for the first , the outcome is prompt splash downstream $\tau = 0.17$, Figure 4.14a. The increase of crossflow velocity will act so that the flow decreases the occurrence secondary dropltes. However, when the deformation of the droplet is transversal, Figure 4.14b, crown splash is observed, $\tau = 0.11$.

4.1.3.4 50% JF - 50% HVO impingement

Figure 4.15 displays the impingement for a 50% JF - 50% HVO droplet with an influencing crossflow of a) $7\mathrm{m.s}^{-1}$ and b) $10\mathrm{m.s}^{-1}$.

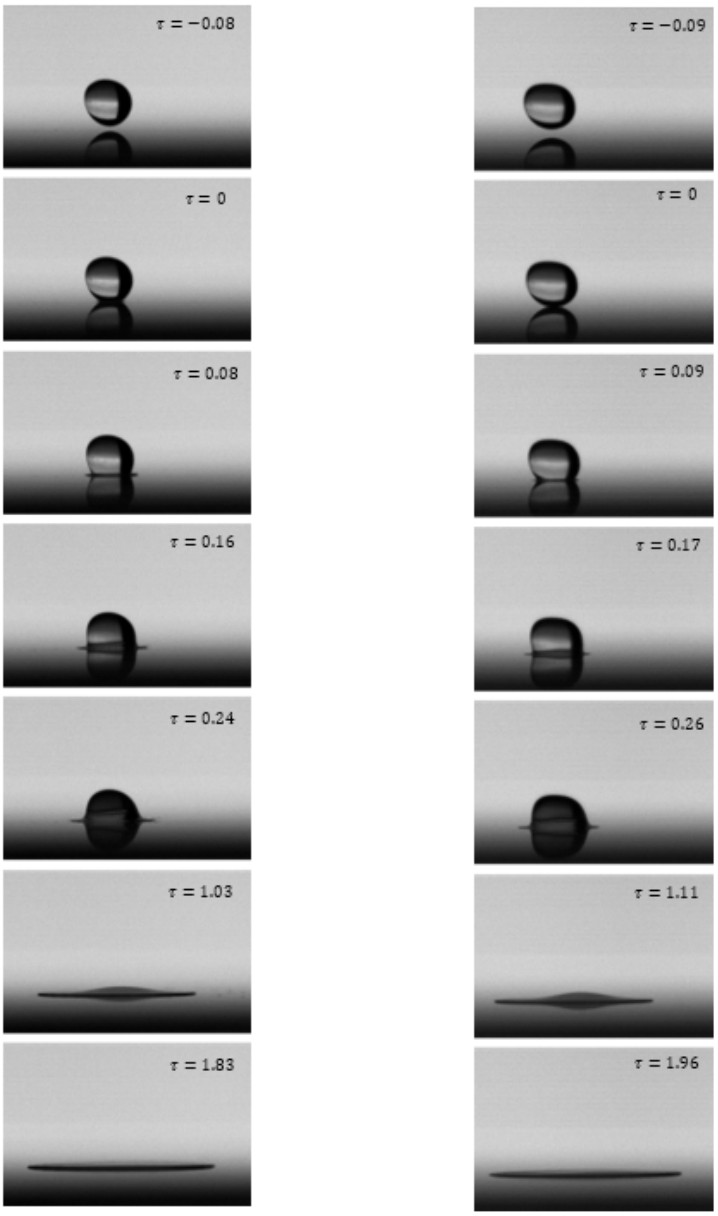

(a) (b)

Figure 4.15: 50% JF - 50% HVO droplet impingement with a crossflow velocity of: a) $7\,\mathrm{m\,s}^{-1}$ and b) $10\,\mathrm{m\,s}^{-1}$.

Figure 4.15a displays the development of impingement of a droplet of 50% JF - 50% HVO under the influence of a crossflow of $\mathrm{U_{cf}} = 7\mathrm{m.s}^{-1}$. Here, after the moment of impact, it is possible

to notice the development of prompt splash downstream, $\tau = 0.16$. This tiny droplets build up while the lamella spreads, moving in the direction of the flow, $\tau = 1.03$.

When the crossflow velocity is increased to $\mathrm{U_{cf}} = 10\mathrm{m.s^{-1}}$, no secondary atomization occurs, $\tau = 0.17$. Similar to the case stated in section 4.1.3.2, the flow acts to smooth the small droplets, suppressing the prompt splash.

4.2 Splash-Threshold

As described in the bibliographic contextualization, several criteria were presented in order to establish the transition between deposition and splash regimes. In this chapter are presented the results obtained for each impact condition.

The first subsection is devoted to the normal impact and the second is dedicated to the crossflow impact. The objective of this study is to verify the experimental results with the empirical correlations.

4.2.1 Normal Impact

The transition between deposition and splash is presented, in this subsection, for the normal impact and for each fluid studied. The drops' absolute velocity is increased by increasing the impact height (needle to surface height). Table 4.1 represents the parameters inherent for each fluid deposition/splash transition such as impact velocity, droplet diameter and non-dimensional numbers.

Table 4.1: Deposition/splash threshold for normal impact.

	100% JF		75% JF - 25% HVO		50% JF - 50% HVO		H_2O	
Regime	Deposition	Splash	Deposition	Splash	Deposition	Splash	Deposition	Splash
$\mathrm{D_0}[mm]$	3.0		3.1		3.1		4.1	
$\mathrm{U_0}[m.s^{-1}]$	1.7	1.9	1.9	2.2	1.7	1.8	2.2	2.4
We	262	328	337	478	293	331	286	340
Re	3563	3987	3198	3808	2349	2496	9190	10018
$\mathrm{Oh}.10^3$	4.5		5.7		7.3		1.8	
La	48475		30307		18850		298480	
Ca	0.07	0.08	0.11	0.13	0.12	0.13	0.03	0.03
Bo	2.8		2.9		3.0		2.3	
Fr	94	118	115	163	97	109	125	149

The dynamic behaviour of a droplet impinging onto a surface is mainly dependent on the physical properties of the fluid. Once droplet diameter between the mixtures differs due to surface tension, a greater surface tension means a greater diameter for the same injection needle.

The droplet initial diameter has a direct influence on the impact velocity needed for the occurrence of splash. As expected, $\mathrm{H_2O}$ requires a higher velocity for the transition between deposition and splash. Although the jet fuel mixtures present the same diameter, their surface tension diverges enough to alter the transition velocity. Therefore, 75% JF - 25% HVO transition velocity is higher than 100% JF, in its turn is higher than 50% JF - 50%HVO.

As referred above, three criteria are used to verify the experimental results. According to ref. [17], for a dry surface, the splash threshold takes' into consideration the A coefficient, which depends on the surface roughness (Ra). Using a equation developed by ref. [5] that interpolates the data provided in table 2.2 to obtain the correct value for A (approximately $\mathrm{A} = 4193$ for Ra $= 0.19\,\mu\mathrm{m}$. Therefore, the criteria translates into:

$$We_c = 4193.La^{-0.18} \quad (4.1)$$

In order to compare the results with other criteria, ref. [5] transformed the Weber and Laplace numbers in to Reynolds and Ohnesorge numbers respectively. The equation is presented as:

$$Oh.Re^{1.218} = A^{0.6097} \quad (4.2)$$

Two more criteria were used to verify the experimental results with the empirical correlation, [11, 37]. The equations regarding these thresholds are presented in section 2.4 and only depend on Reynolds and Ohnesorge numbers.

Ref. [11] proposed a splashing threshold based on the correlation presented below. In their experiments, the authors used a rotation disk in order to create the air boundary layer.

$$K_c = Oh.Re^{1.25} = 57.7 \quad (4.3)$$

Ref. [37] determined an empirical correlation for the deposition/splash transition using Oh and Re numbers, presented as:

$$K_c = Oh.Re^{0.609} = 0.85 \quad (4.4)$$

In Figure 4.16 is displayed the experimental results obtained for the deposition/splash transition for normal impact compared to the empirical correlations proposed by refs. [11, 17, 37]. Each fluid has a different symbol, and when the symbol is filled, splash occurs. Regarding the mixtures, it is possible to notice that the transition between non-splash/splash fits well for the correlation proposed by [37]. However, both 100% JF and $\mathrm{H_2O}$ are plotted in the deposition area where the $\mathrm{H_2O}$ approaches the correlation presented by ref. [17]. Regarding the criteria

proposed by ref. [11], all of the present experimental results are found in the splash region proposed by the authors. One of the reasons for this to happen is the fact that, in their experiments a rotating disk is used which will alter the conditions of impact. Consequently, the drops will impact the surface with a certain angle.

Both the criteria proposed by refs. [17, 37] provide a great adjustment for all the fluids, since all the results seem to follow a similar tendency. Ref. [37] used an aluminium disk with a mean surface roughness of less than $10\,\mathrm{nm}$, which could explain the proximity of the experimental results with their correlation.

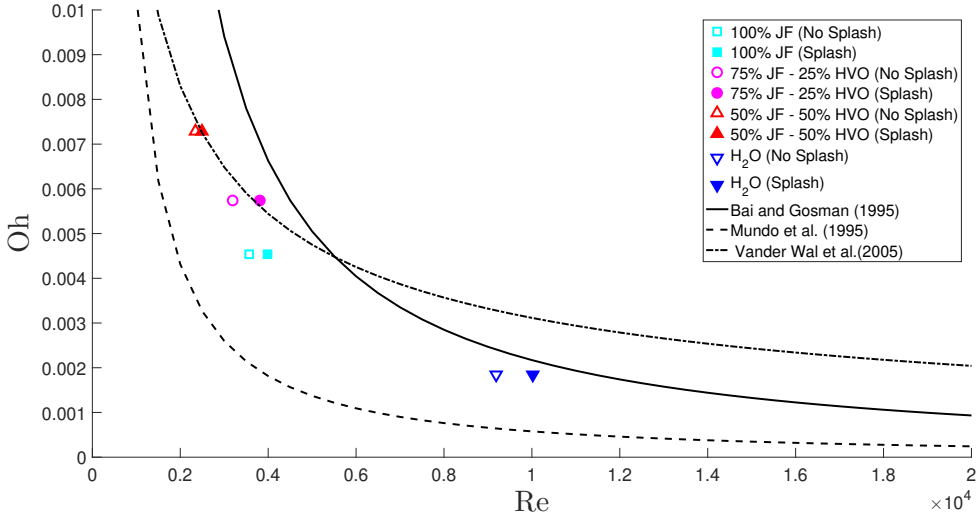

Figure 4.16: Deposition/splash transition results for normal impact plotted against proposed correlations.

4.2.2 Impact with Crossflow

As previously mentioned in the literature, the crossflow may deform the droplet, creating an impact angle (θ) defined as the angle formed between the impact surface and the absolute velocity of the droplet. The following results will present three types of velocity, which are the absolute velocity (U), normal velocity ($\mathrm{U_n}$) and tangential velocity ($\mathrm{U_t}$). Table 4.2 displays the droplets' diameter, impact velocity components and the non-dimensional numbers regarding the impact with a crossflow velocity of $7\,\mathrm{m\,s^{-1}}$.

Once the transition is found for normal impact, and droplet velocity is defined, the crossflow is used to verify the permanence of splash condition. As seen in the experimental results once this crossflow is employed, splash condition is no longer verified for the same impact velocity. Therefore, drop hight release is increased to find the non-splash/splash transition for impact with crossflow. Results show that the impact angle is higher for $\mathrm{H_2O}$ and lower for 100% JF. Within the other two mixtures, the impact angle is higher for 50% JF - 50% HVO than for 75% JF - 25% HVO. It is suggested that an increase of normal velocity will decrease the effect of the crossflow. This was verified for all fluids except for 75% JF - 25% HVO that has a minimal difference. This may occur due to systematic errors from centroid determination and image acquisition, as the difference of tangential velocity is also very small for all of the other fluids.

Table 4.2: Deposition/splash threshold for droplet impact under influence of a $7\,\mathrm{m\,s^{-1}}$ crossflow velocity.

	100% JF		75% JF - 25% HVO		50% JF - 50% HVO		H_2O	
Regime	Deposition	Splash	Deposition	Splash	Deposition	Splash	Deposition	Splash
$D_0[mm]$	3.0		3.1		3.1		4.1	
$U_0[m.s^{-1}]$	2.2	2.3	2.6	2.8	1.9	2.0	2.8	2.9
$U_t[m.s^{-1}]$	1.0	0.9	0.8	0.8	0.5	0.4	0.4	0.3
$U_n[m.s^{-1}]$	2.0	2.1	2.5	2.7	1.8	1.9	2.8	2.9
$\theta[°]$	65		73		76		83	
We	456	498	738	795	356	388	456	468
Re	4703	4915	4729	4909	2599	2704	11663	11813
$Oh.10^3$	4.5		5.7		7.3		1.8	
La	48475		30307		18850		298480	
Ca	0.1	0.1	0.14	0.16	0.14	0.14	0.04	0.04
Bo	2.8		2.9		3.0		2.3	
Fr	165	180	216	271	117	128	201	207

Figure 4.17 presents the experimental data obtained for the deposition/splash transition for an impact with a crossflow velocity of $7\,\mathrm{m\,s^{-1}}$ plotted against the correlations proposed by refs. [11, 17, 37].

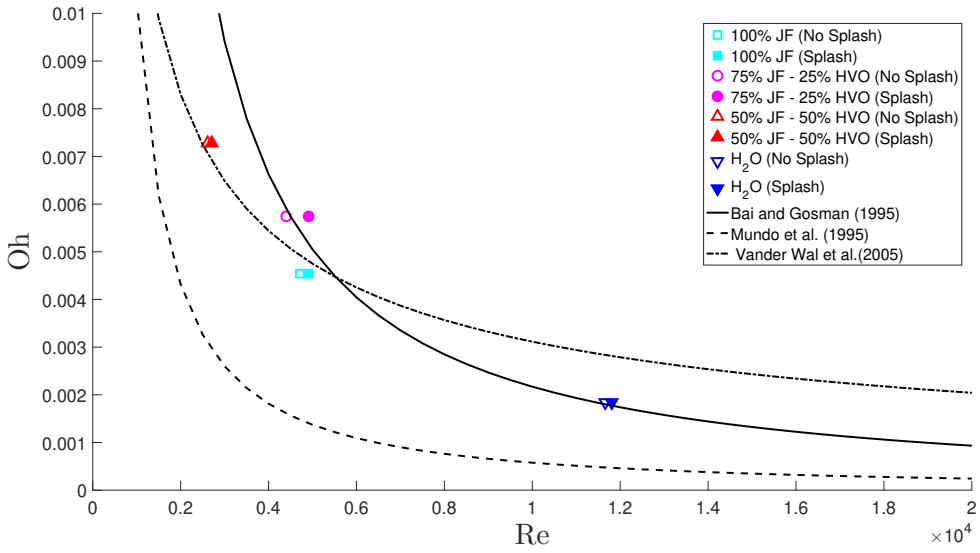

Figure 4.17: Deposition/splash transition results for impact under the influence of $7\,\mathrm{m\,s^{-1}}$ crossflow velocity plotted against proposed correlations.

The criteria that best suits the experimental results are the ones proposed by refs. [17, 37]. The fluids H_2O and 75% JF - 25% HVO fit perfectly in the boundary line for the non-splash/splash transition developed by ref. [17]. However, 50% JF - 50% HVO and 100% JF are plotted on the deposition side of this correlation. For the fluids mentioned before, the line that best suits is the correlation developed by ref. [37], even though both lines fit the 100% JF fluid.

Once more, the criteria developed by ref. [11] presents the least satisfactory correlation for the experimental results obtained. None of the fluids are close to the boundary layer with all of the results plotted in the splashing area. This may be due to the fact that the authors used droplets with a much smaller diameter ($D_0 = 60\,\mu m$ to $150\,\mu m$) than the ones used in this experimental work and the surface characteristics differ from the ones of the present work.

4.3 Summary

In this section, a summary of the results obtained in the experimental work is presented. This study suggests that physical properties of the fluids influence the droplet impact outcome. It was also shown that a higher velocity is needed to induce splash when crossflow is present. The comparison between impact velocities needed for the occurrence of splash for normal impact and crossflow impact are presented in Table 4.3.

Table 4.3: Absolute velocity for splash occurrence regarding the normal impact (NI) and impact with a crossflow (CI) of $7 m.s^{-1}$.

$U[m.s^{-1}]$	100% jet fuel	75% jet fuel - 25% HVO	50% jet fuel - 50% HVO	H_2O
NI	1.9	2.2	1.8	2.4
CI	2.3	2.8	2.0	2.9

Regarding the criteria used to compare the experimental results with empirical correlations, a pattern is observed. For normal impact, the empirical correlation developed by ref. [17] does not suit the results obtained and the criteria developed by ref. [37] accurately fits the results obtained for the fluid mixtures. However, the results obtained have the same decreasing tendency of the correlation proposed by ref. [17].

Regarding the impact with crossflow, once again, the empirical correlation proposed by ref. [17] suits perfectly the results obtained for H_2O and for the results obtained for 75% JF - 25% HVO. The results for 100% JF seem to fit this boundary as well. For 50% JF - 50% HVO the correlation that best fits is the one proposed by ref. [37]. However, this criterion seems to also fit the results for 100% JF.

The criteria proposed by ref. [11] does not suit any of the impact conditions, with all of the results spotted in the splash area.

Respecting the crossflow variation study, it began with applying the same impact velocity in which splash first occurred, in each fluid, for $U_{cf} = 7 m.s^{-1}$, following an increase of crossflow velocity. Four crossflow velocities were studied: $7 m.s^{-1}$, $10 m.s^{-1}$, $12 m.s^{-1}$ and $15 m.s^{-1}$. For the jet fuel mixtures breakup occurred at $U_{cf} = 13 m.s^{-1}$ and for H_2O occurred at $U_{cf} = 18.5 m.s^{-1}$. Table 4.4 presents the resulting outcomes and is not intended for comparison between fluids. As stated in the previous section, five regimes were observed: prompt splash (PS), corona splash (CS), deposition (D), prompt-corona splash (PS-CS) and breakup (B). It is important to mention that, due to droplet deformation, the phenomena obtained were asymmetric.

Results suggest that an increase of crossflow velocity allied with the droplet deformation could act in a way to decrease the occurrence of splash or even inhibit it. In the cases prompt splash was observed for $\mathrm{U_{cf}} = 7\mathrm{m.s^{-1}}$, the transversal flow inhibited the splash and no secondary atomization was observed. In the case where corona splash is observed, the increasing crossflow velocity gradually decreases the splash occurrence.

Table 4.4: Influence of the crossflow on impact outcome.

Fluid	$7\mathrm{m.s^{-1}}$	$10\mathrm{m.s^{-1}}$	$12\mathrm{m.s^{-1}}$	$15\mathrm{m.s^{-1}}$
$\mathrm{H_2O}$	PS	D	D	PS
100% JF	PS	D	D	B
75% JF - 25% HVO	CS	PS-CS	PS/ PS-CS	B
50% JF - 50% HVO	PS	D	D	B

Chapter 5

Conclusions and Future Work

5.1 Conclusions

This work was dedicated to the study of the dynamic behaviour of a single droplet impinging onto a dry surface under the influence of an increasing crossflow velocity. The main objective was to understand the influence of the crossflow on droplet impact outcome. For this, and in order to study the effect of each velocity component, two major studies were made: the study of the differences between non-splash/splash transition for normal impact and crossflow impact to understand the influence of the normal velocity component, and the study of the influence of crossflow variation to perceive the effect of the tangential velocity component. When an impinging droplet is under the effect of a crossflow, it is susceptible to a certain deformation. However, when a droplet impacts normally to the surface it is spherical. This difference varies the impact outcome.

Four fluids were considered in this experimental work: 100% JF, 75% JF - 25% HVO, 50% JF - 50% HVO and $\mathrm{H_2O}$ (pure water) as a reference fluid, since all its properties are well described in the literature. The study of droplet impact regarding 100% JF and $\mathrm{H_2O}$ is already reported in the literature, however, there are only a few studies regarding Jet-Fuel mixtures with Bio-fuel. Concerning the impact surface, a smooth aluminium plate was used with a mean surface roughness of $\mathrm{Ra} = 0.19\,\mu\mathrm{m}$.

In a first approach, the visualization of the outcomes of a droplet impinging onto a dry surface was made. The results obtained are consistent with those present in the literature contextualization, where three outcomes were observed for normal impact: spread, fingering and prompt splash; and four were seen for crossflow impact: spread, fingering, prompt splash and corona splash. When analysing the impact velocities, results suggest that the vertical velocity required to the occurrence of splash is greater for crossflow impact than for normal impact. In this way, a study of the splashing threshold was made for both impacts. It is observed that the surface tension, viscosity and density have a direct influence on droplet size and impact phenomena.

The results obtained were, then, compared with empirical correlations proposed in the literature. For both impact conditions, the empirical correlation proposed by refs. [17, 37] were the ones that better suit the results obtained in this experimental study. On the contrary, in the criteria proposed by ref. [11], the experimental data is plotted in the splashing area. This may due to the fact that, in their experiments, the authors used a rotating disk and significantly smaller droplets.

The impact velocity was divided into two components to study the influence of each one in the impact outcome. In this way, a study of the variation of crossflow velocity was made . Using the same initial condition, i.e. the normal velocity where splash first occurs for a crossflow velocity of $\mathrm{U_{cf}} = 7\mathrm{m.s^{-1}}$, the crossflow velocity was increased until breakup occurred. For jet fuel and mixtures, breakup occurred at $\mathrm{U_{cf}} = 13\mathrm{m.s^{-1}}$ and for $\mathrm{H_2O}$ occurred at $\mathrm{U_{cf}} = 18.5\mathrm{m.s^{-1}}$. Through the visualization of the effect of this velocity variation, the phenomena inherent to

crossflow impact were observed. However, results suggest that this augmentation acts in a way to decrease the occurrence of splash or even inhibit it.

Regarding the behaviour of the fluids used, it was noticeable the influence of the biofuel in the final results. The mixtures presented different performances when compared to the conventional Jet A-1 and $\mathrm{H_2O}$.

The studies of the effect of a crossflow variation on mixed jet fuel droplet impingement are scarce, thus, a continue investigation is needed in order to understand the mechanisms promoting the different phenomena.

5.2 Future Work

The extension of experimental data is important for the verification of present results, thus the study of a wide range of droplet diameters and Ohnesorge variation is important to verify the tendencies and compare with the empirical correlations, since droplet diameter affects directly the threshold velocities and, consequently, impact outcomes. Each velocity component must be study in order to verify the significance on impact outcome and on splashing threshold.

It is also of importance to study the influence of the variation of surface roughness on impact outcomes and the distribution of secondary atomization. It would be of interest to study different mixtures in order to better understand the influence of biofuel.

There is still lack of studies focused on impacts with a crossflow. The in-depth study of the threshold for different crossflow velocities could prove to be valuable in understanding the influence of crossflow on impact outcomes and droplets' spatial distribution.

Bibliography

[1] ASTM D1655, *Standard Specification for Aviation Turbine Fuels*. American Society For Testing and Materials, 2015.

[2] ASTM D7566, *Standard Specification for Aviation Turbine Fuel Containing Synthesized Hydrocarbons*. American Society for Testing and Materials, 2016.

[3] B. Pizziol, "Design and experimental characterization of an air-assisted, impinging-jets atomizer for aeronautical aplications with biofuel." Master's thesis, Politectino di Milano, Scuola di Ingegneria Industriale e dell'Informazione, 2016.

[4] R. D. Deegan, P. Brunet, and J. Eggers, "Complexities of splashing," *Nonlinearity*, vol. 21, no. 1, pp. C1–C11, dec 2007.

[5] I. Ferrão, "Dynamic behavior of a single droplet impinging onto a sloped surface," Master's thesis, Universidade da Beira Interior, 2018.

[6] Jayaratne and Mason, *The Coalescence and Bouncing of Water Drops at an Air/Water Interface*, 1964.

[7] Yao and Cai, "The dynamics and leidenfrost temperature of drops impacting on a hot surface at small angles," vol. 1, no. 4. Elsevier BV, oct 1988, pp. 363–371.

[8] Š. Šikalo, C. Tropea, and E. Ganić, "Dynamic wetting angle of a spreading droplet," *Experimental Thermal and Fluid Science*, vol. 29, no. 7, pp. 795–802, aug 2005.

[9] R. Rioboo, C. Tropea, and M. Marengo, "Outcomes from a drop impact on solid surfaces," *Atomization and Sprays*, vol. 11, no. 2, p. 12, 2001.

[10] C. D. Stow and M. G. Hadfield, "An experimental investigation of fluid flow resulting from the impact of a water drop with an unyielding dry surface," *Proceedings of the Royal Society A: Mathematical, Physical and Engineering Sciences*, vol. 373, no. 1755, pp. 419–441, jan 1981.

[11] C. Mundo, M. Sommerfeld, and C. Tropea, "Droplet-wall interactions: Experimental studies of the deformation and breakup process," *International Journal of Multiphase Flow*, vol. 21, no. 2, pp. 151–173, apr 1995.

[12] A. S. Moita and A. L. N. Moreira, "Influence of surface properties on the dynamic behavior of impacting droplets," 2018.

[13] C. Mundo, M. Sommerfeld, and C. Tropea, "On the modeling of liquid sprays impinging on surfaces," *Atomization and Sprays*, vol. 8, no. 6, pp. 625–652, 1998.

[14] A. Yarin, "Drop impact dynamics: Splashing, spreading, receding, bouncing…," *Annual Review of Fluid Mechanics*, vol. 38, no. 1, pp. 159–192, jan 2006.

[15] M. Rein, "Phenomena of liquid drop impact on solid and liquid surfaces," *Fluid Dynamics Research*, vol. 12, no. 2, pp. 61–93, aug 1993.

[16] A. M. Worthington, "On the forms assumed by drops of liquids falling vertically on a horizontal plate," *Proceedings of the Royal Society of London*, vol. 25, no. 171-178, pp. 261–272, jan 1876.

[17] Bai and Gosman, “Development of methology for spray impingement simulation,” 1995.

[18] C. Josserand and S. Thoroddsen, “Drop impact on a solid surface,” *Annual Review of Fluid Mechanics*, vol. 48, no. 1, pp. 365–391, jan 2016.

[19] I. V. Roisman, R. Rioboo, and C. Tropea, “Normal impact of a liquid drop on a dry surface: Model for spreading and receding,” *Proceedings of the Royal Society of London. Series A: Mathematical, Physical and Engineering Sciences*, vol. 458, no. 2022, pp. 1411–1430, jun 2002.

[20] P. Tsai, M. H. W. Hendrix, R. R. M. Dijkstra, L. Shui, and D. Lohse, “Microscopic structure influencing macroscopic splash at high weber number,” *Soft Matter*, vol. 7, no. 24, p. 11325, 2011.

[21] S. T. Thoroddsen and J. Sakakibara, “Evolution of the fingering pattern of an impacting drop,” *Physics of Fluids*, vol. 10, no. 6, pp. 1359–1374, jun 1998.

[22] M. Broumand and M. Birouk, “Liquid jet in a subsonic gaseous crossflow: Recent progress and remaining challenges,” *Progress in Energy and Combustion Science*, vol. 57, pp. 1–29, nov 2016.

[23] A. Mashayek and N. Ashgriz, “Atomization of a liquid jet in a crossflow,” in *Handbook of Atomization and Sprays*. Springer US, dec 2010, pp. 657–683.

[24] M. Herrmann, “The influence of density ratio on the primary atomization of a turbulent liquid jet in crossflow,” *Proceedings of the Combustion Institute*, vol. 33, no. 2, pp. 2079–2088, jan 2011.

[25] R. Ragucci, A. Bellofiore, and A. Cavaliere, “Breakup and breakdown of bent kerosene jets in gas turbine conditions,” *Proceedings of the Combustion Institute*, vol. 31, no. 2, pp. 2231–2238, jan 2007.

[26] M. Broumand, M. M. Ahmed, and M. Birouk, “Experimental investigation of spray characteristics of a liquid jet in a turbulent subsonic gaseous crossflow,” *Proceedings of the Combustion Institute*, vol. 37, no. 3, pp. 3237–3244, 2019.

[27] A. Silva, “Experimental and numerical study of physical aspects of fuel processes,” Ph.D. dissertation, Universidade da Beira Interior, 2007.

[28] T. Kékesi, G. Amberg, and L. P. Wittberg, “Corrigendum to: “drop deformation and breakup”. int. j. multiphase flow, 66, (2014) 1–10.” *International Journal of Multiphase Flow*, vol. 93, pp. 213–215, jul 2017.

[29] D. R. Guildenbecher, C. López-Rivera, and P. E. Sojka, “Secondary atomization,” *Experiments in Fluids*, vol. 46, no. 3, pp. 371–402, jan 2009.

[30] G. Carrolo, D. Ribeiro, J. M. Barata, and A. R. Silva, “Aerodynamic breakup of a single droplet due to a crossflowed airstream,” in *AIAA Scitech 2019 Forum*. American Institute of Aeronautics and Astronautics, jan 2019.

[31] Cunha, N., Ribeiro, D., Barata, J., and Silva, A., “The splash deposition transition limits of a biofuel droplet wall impact with a and without crossflow,” in *ICLASS 2018, 14 th Triennial International Conference on Liquid Atomization and Spray Systems, Chicago, IL, USA*, July 22-26, 2018.

[32] C. Rodrigues, “Modelling of spray-wall and impingement,” Ph.D. dissertation, Universidade da Beira interior, 2016.

[33] M. R. O. Panão, A. L. Moreira, and D. F. Durão, “Effect of a cross-flow on spray impingement with port fuel injection systems for HCCI engines,” *Fuel*, vol. 106, pp. 249–257, apr 2013.

[34] M. R. O. Panao and A. L. N. Moreira, “Experimental characterization of an intermittent gasoline spray impinging under cross-flow conditions,” *Atomization and Sprays*, vol. 15, no. 2, pp. 201–222, 2005.

[35] I. Ferrao, D. Ribeiro, J. M. Barata, and A. R. Silva, “Comparative study of droplet impact onto sloped surface versus a droplet impact onto a surface with a crossflow,” in *AIAA Scitech 2019 Forum*. American Institute of Aeronautics and Astronautics, jan 2019.

[36] N. Cunha, “Experimental study of a single droplet imping on a dry surface with and without a crossflow: Jet fuel and biofuel mixtures,” Master’s thesis, Universidade da Beira Interior, 2018.

[37] R. L. V. Wal, G. M. Berger, and S. D. Mozes, “The splash/non-splash boundary upon a dry surface and thin fluid film,” *Experiments in Fluids*, vol. 40, no. 1, pp. 53–59, oct 2005.

[38] D. Ribeiro, “Experimental study of a single droplet impinging upon liquid films: Jet fuel and biofuel mixtures,” Master’s thesis, Universidade da Beira Interior, 2018.

[39] Metha and Bradshaw, “Design rules for small low speed wind tunnels,” *Aeronautical Journal*, 1979.

[40] G. Carrolo, “Aerodynamic breakup of a single droplet due to crossflow,” Master’s thesis, Universidade da Beira Interior, 2019.

[41] Coordinating Research Council, *Handbook of Aviation Fuel Properties*. The council, 1983.

[42] H. Almohammadi and A. Amirfazli, “Understanding the drop impact on moving hydrophilic and hydrophobic surfaces,” *Soft Matter*, vol. 13, no. 10, pp. 2040–2053, 2017.

Annex

Publications

Leal, F., Ferrão I., Silva, A. and Barata, J., Jet Fuel and Biofuel Droplets Impinging Onto a Dry Surface, in: 14th International Conference on Energy for a Clean Environment, September 8-12, 2019, Funchal, Madeira, Portugal.

Leal, F., Ferrão I., Silva, A. and Barata, J., Effect of Crossflow Variation On a Single Droplet Impinging onto Dry Surface, in : AIAA Aerospace Sciences Meeting, January 6-10, 2020, Orlando, Florida, USA. [Submitted]

14th International Conference on Energy for a Clean Environment
September 8-12, 2019, Funchal, Madeira, Portugal

JET FUEL AND BIOFUEL DROPLETS IMPINGING ONTO A DRY SURFACE: EFFECT OF CROSSFLOW VARIATION

Filipa Leal*, Inês Ferrão*, André Silva* and Jorge Barata*

* AEROG-LAETA, Universidade da Beira Interior, Covilhã, 6200-001, Portugal
E-mail:andre@ubi.pt

ABSTRACT

The actual environmental concerns require an immediate demand for the use of clean energies. Nowadays, the negative impact of the aeronautical sector on greenhouse gas and pollutants emissions forced humans to adapt and find more efficient and ecological solutions. The introduction of biofuels in fuel mixtures for aircraft engines is one of the starting points. In this way, several efforts must be made in order to incorporate them in commercial aviation successfully. To understand the behaviour of jet fuel and biofuel mixtures, it was considered a combination of conventional jet fuel
(Jet A1) and a biofuel (HVO - Hydroprocessed Vegetable Oil) and four fluids were used: 100% jet fuel, 75% jet fuel 25% HVO, 50% jet fuel - 50% HVO and H_2O (pure water) as a reference. Since the current legislation allows a minimum concentration of 50% in volume of jet fuel, no other mixtures were considered for this study. To achieve the conditions necessary for the study of droplet impingement, an experimental facility was used with a dry, smooth aluminium impact surface.
The main objective of this experimental study is understanding the influence of crossflow variation on droplet impact outcomes. When a droplet is influenced by a crossflow, it may deform asymmetrically, oscillate and be oriented by the gas flow, affecting the impact phenomena. Comparing the impact velocities for normal and crossflow impacts, the results suggest that a higher velocity is needed to induce splash in the presence of crossflow. This occurrence was verified for all the fluids. Regarding fuel mixtures, it was noticed that the percentage of biofuel influences the impact outcome. Subsequently, the splashing threshold was analyzed and defined for normal and crossflow impact. It was also crucial to study the crossflow variation effect on droplet deformation and outcome. Different crossflow velocities (Ucf) were tested, such as U_{cf} = 7m/s , U_{cf} = 10m/s , U_{cf} = 12m/s and U_{cf} = 15m/s. For 100% jet fuel and fuel mixtures, aerodynamic breakup occurred for U_{cf} = 13m/s and, for H_2O, it occurred for U_{cf} = 18.5m/s. The results obtained suggest that an increase of tangential velocity, allied with the droplet deformation, act in a way to decrease the magnitude of splash or even inhibit it.

***Keywords**: Jet-Fuel, Biofuel, Crossflow, Secondary atomization*

Effect of Crossflow Variation On a Single Droplet Impinging onto a Dry Surface

Filipa Leal*, Inês Ferrão†, André Silva‡ and Jorge Barata§
Universidade da Beira Interior, Covilhã, 6200-001, Portugal

Extended Abstract

The phenomena of droplet impingement have several applications in engineering and industrial processes. High-speed impacts can cause erosion in steam turbines, and the impact of fuel sprays on internal combustors walls affects the rate of fuel evaporation, thus, influencing the combustion efficiency. Several studies were made in order to understand normal droplet impingement for water, glycerine mixtures and ethanol, where the surface is stationary and the phenomena are symmetric [1–4]. Injection of a liquid jet in a gaseous crossflow is one of the most efficient spray generation techniques when rapid mixing is desired. When a droplet is affected by a crossflow, it may deform and rotate due to aerodynamic forces applied to it. This flow will also apply additional force to the drop, which can vary the outcome of impingement [5–9]. The current work is focused in using fuel mixtures of jet fuel (Jet A1) and HVO (Hydroprocessed Vegetable Oil) biofuel (NEXBTL) in order to draw the comparison between these fuel mixtures and conventional jet fuel.

The main objective of this experimental work is to understand the influence of a crossflow on droplet impact outcome. For this, and in order to study the effect of each velocity component, two major studies were made: the study of the differences between non-splash/splash transition for normal impact and crossflow impact to understand the influence of the normal velocity component, and the study of the influence of crossflow velocity variation to perceive the effect of the tangential velocity component. To achieve the necessary conditions for the present work, an experimental facility was used to study the main parameters that influence droplet impact phenomena. The experimental arrangement is composed by an impact surface (a dry, smooth aluminium plate with a mean roughness of 0.19 μm), a wind tunnel, a system for image acquisition, a droplet dispersing system and a LED (Light Emitting Diode) illumination set. The experiments were conducted with different crossflow velocities and four fluids: 100% jet fuel, 75% jet fuel - 25%HVO, 50% jet fuel - 50%HVO and H_2O, being the later one used as reference fluid because of its well-known properties. The droplet diameter of these fluids is, approximately, 3mm for the fuel mixtures and 100% jet fuel and 4mm for H_2O [10, 11]. As the current legislation only permits the use of a minimum of 50% in volume for Jet A1 for commercial aviation, no other fuel mixtures were considered for the present work [12, 13].

At the moment of impact, a drop may be spherical or elliptical, the impact can be perpendicular or oblique and occur in air and vacuum. The surface can be hard or soft, rough or smooth and dry or wet [14]. Consequently, the outcome of droplet impact on a solid surface depends on the properties of the liquid such as density (ρ), viscosity (μ) and surface tension (σ), surface conditions and impact angle. The fluid properties used in this experimental study are listed in the work developed by Ref. [10].

In a first approach, the visualization of the outcomes produced by droplet impingement was made. Three outcomes were observed for normal impact: spread, fingering and prompt splash; and five were identified for crossflow impact: spread, fingering, prompt splash, corona splash and breakup. Spread refers to an impact in which the droplet spreads out, without forming secondary atomization. Fingering occurs when the lamella suffers disturbances during the spreading phase in the outer rim, whose growth results in finger-like shapes. Prompt splash occurs for high Weber and Reynolds numbers, and the impact generates small droplets that are ejected from the impact region. Corona splash is observed when a drop impacts with sufficient velocity, so the outer rim formed by the lamella has enough energy that elevates and creates a crown-like shape. This corona later disintegrates, producing secondary atomization. Aerodynamic breakup occurs when, due to deformation caused by the flow, the droplet disintegrates before reaching the surface [2, 14].

To determine the impact velocity an algorithm previously developed by Ref. [15], on MATLAB®Software, was used. Once the study of normal impact was concluded, the crossflow (U_{cf} = 7m.s^{-1}) study was started. The minimum impact velocities needed for the occurrence of splash for normal impact and crossflow impact are presented in Table 1.

*Master Student, Aerospace Sciences Department, filipaleal02@gmail.com.
†Ph.D. Student, Aerospace Sciences Department, ines_ferrao_abril_11@hotmail.com.
‡Assistant Professor, Aerospace Sciences Department, and Member of AIAA, andre@ubi.pt.
§Full Professor, Aerospace Sciences Department, and Associate Fellow of AIAA, jmmbarata@gmail.com.

Table 1 Impact velocity for the first splash occurrence regarding the normal impact (NI) and impact with crossflow (CI) of $7\,\mathrm{m\,s^{-1}}$.

$U[m.s^{-1}]$	100% jet fuel	75% jet fuel - 25% HVO	50% jet fuel - 50% HVO	H_2O
NI	1.9	2.2	1.8	2.4
CI	2.3	2.8	2.0	2.9

One is able to perceive that the H_2O fluid requires a higher impact velocity for the occurrence of splash for both impact conditions, which is caused by its surface tension. Although the fuel mixtures and 100% jet fuel present the same diameter, the splash phenomenon occurs for different impact velocities. Therefore, biofuel properties influence the impact outcome, in this way, 75% jet fuel - 25% HVO requires a higher velocity than 100%jet fuel and in its turn is higher than 50% jet fuel - 50% HVO. Results suggest that a higher impact velocity is needed to induce splash when crossflow is present.

A study of the splashing threshold was, then, made for both impact conditions and the results obtained were compared with empirical correlations proposed in the literature [1, 4, 16]. For normal impact it was observed that the results obtained in this experimental work have the same tendency of the non-splash/splash transition criterion proposed by Ref.[1]. For crossflow impact, the empirical correlation proposed by Ref. [4] provided a great adjustment for all the fluids. The criterion proposed by Ref. [16] did not suit any of the impact conditions, with all of the results spotted in the splash area.

When a droplet is influenced by a crossflow, the impact velocity has two components: normal velocity component and tangential velocity component. To study the influence of the tangential component of velocity it was performed a crossflow velocity variation study. Four velocities were studied: $7\mathrm{m.s^{-1}}$, $10\mathrm{m.s^{-1}}$, $12\mathrm{m.s^{-1}}$, $15\mathrm{m.s^{-1}}$. For the fuel mixtures and 100% jet fuel breakup occurred at a crossflow velocity (U_{cf}) of $13\mathrm{m.s^{-1}}$ and for H_2O occurred at $U_{cf} = 18.5\mathrm{m.s^{-1}}$. The study began with applying the same impact velocity in which splash occurred, in each fluid, for $U_{cf} = 7\mathrm{m.s^{-1}}$, following an increase of crossflow velocity. Table 2 presents the resulting outcomes and is not intended for comparison between fluids. The outcomes observed were prompt splash (PS), corona splash (CS), deposition (D), prompt-corona splash (PS-CS) and breakup (B). It is important to mention that, due to droplet deformation, the phenomena obtained were asymmetric. Results suggest that an increase of tangential velocity allied with the droplet deformation could act in a way to decrease the magnitude of splash or even inhibit it. In the cases prompt splash was observed for $U_{cf} = 7\mathrm{m.s^{-1}}$, the transversal flow inhibited the splash and no secondary atomization was observed. In the case where corona splash is observed, the tangential velocity gradually decreases the splash magnitude.

Table 2 Influence of the crossflow on impact outcome.

Fluid	$7\mathrm{m.s^{-1}}$	$10\mathrm{m.s^{-1}}$	$12\mathrm{m.s^{-1}}$	$15\mathrm{m.s^{-1}}$
100% jet fuel	PS	D	D	B
75% jet fuel - 25% HVO	CS	PS-CS	PS/ PS-CS	B
50% jet fuel - 50% HVO	PS	D	D	B
H_2O	PS	D	D	PS

Figure 1 displays the development of impingement for a 100% jet fuel droplet with a crossflow velocity of a) $7\,\mathrm{m\,s^{-1}}$ and b) $10\,\mathrm{m\,s^{-1}}$. Before the moment of impact, the droplet is deformed and for Figure1 a) is possible to notice the development of prompt splash downstream. These tiny droplets build up while the lamella spreads, moving in the direction of the flow. Figure 1 b) displays the development of the same fluid but, influenced by a crossflow velocity of $U_{cf} = 10\mathrm{m.s^{-1}}$. Due to the shear forces and internal flow of the droplet, this droplet is deformed in a way that the side is flatten, resulting in a cap-shape geometry. After the moment of impact, the droplet spreads and no secondary atomization is observed.

In Figure 2 is presented the impinging development of a 75% jet fuel - 25% HVO droplet with an influencing crossflow of a) $7\,\mathrm{m\,s^{-1}}$ and b) $10\,\mathrm{m\,s^{-1}}$. When the droplet impacts the surface is possible to perceive the formation of an asymmetric corona splash. However, when the same fluid droplet is under the influence of a crossflow velocity of $U_{cf} = 10\mathrm{m.s^{-1}}$, the increasing of tangential velocity smooths the secondary droplets upstream and prompt-corona splash occurs.

Figure 3 presents the impinging development of the same fluid droplet mentioned before but influenced by a crossflow velocity of $12\,\mathrm{m\,s^{-1}}$, being possible to notice that the droplet deformation has a great influence on impact outcome.

The studies of the effect of a crossflow variation on mixed jet fuel droplet impingement are scarce, thus, a continue investigation is needed to understand the mechanisms promoting the different phenomena.

Acknowledgments

The present work was performed under the scope of the Aeronautics and Astronautics Research Center (AEROG) of the Laboratório Associado em Energia, Transportes e Aeronáutica (LAETA) activities and it was supported by Fundação para a Ciência e Tecnologia (FCT) through the project number UID/EMS/6022/2019.

References

[1] Bai, and Gosman, "Development of methology for spray impingement simulation," 1995.

[2] Rioboo, R., Tropea, C., and Marengo, M., "Outcomes from a drop impact on solid surfaces," *Atomization and Sprays*, Vol. 11, No. 2, 2001, p. 12. doi:10.1615/atomizspr.v11.i2.40.

[3] Worthington, A. M., "On the Forms Assumed by Drops of Liquids Falling Vertically on a Horizontal Plate," *Proceedings of the Royal Society of London*, Vol. 25, No. 171-178, 1876, pp. 261–272. doi:10.1098/rspl.1876.0048.

[4] Wal, R. L. V., Berger, G. M., and Mozes, S. D., "The splash/non-splash boundary upon a dry surface and thin fluid film," *Experiments in Fluids*, Vol. 40, No. 1, 2005, pp. 53–59. doi:10.1007/s00348-005-0045-1.

[5] Silva, A., "Experimental and Numerical Study of Physical Aspects of Fuel Processes," Ph.D. thesis, Universidade da Beira Interior, 2007.

[6] Broumand, M., and Birouk, M., "Liquid jet in a subsonic gaseous crossflow: Recent progress and remaining challenges," *Progress in Energy and Combustion Science*, Vol. 57, 2016, pp. 1–29. doi:10.1016/j.pecs.2016.08.003.

[7] Mashayek, A., and Ashgriz, N., "Atomization of a Liquid Jet in a Crossflow," *Handbook of Atomization and Sprays*, Springer US, 2010, pp. 657–683. doi:10.1007/978-1-4419-7264-4_29.

[8] Rein, M., "Phenomena of liquid drop impact on solid and liquid surfaces," *Fluid Dynamics Research*, Vol. 12, No. 2, 1993, pp. 61–93. doi:10.1016/0169-5983(93)90106-k.

[9] Kékesi, T., Amberg, G., and Wittberg, L. P., "Corrigendum to: "Drop deformation and breakup". Int. J. Multiphase Flow, 66, (2014) 1–10." *International Journal of Multiphase Flow*, Vol. 93, 2017, pp. 213–215. doi:10.1016/j.ijmultiphaseflow.2016.02.002.

[10] Cunha, N., "Experimental study of a single droplet imping on a dry surface with and without a crossflow: jet fuel and biofuel mixtures," Master's thesis, Universidade da Beira Interior, 2018.

[11] Ribeiro, D., "Experimental Study of a Single Droplet Impinging upon Liquid Films: Jet Fuel and Biofuel Mixtures," Master's thesis, Universidade da Beira Interior, 2018.

[12] ASTM D1655, *Standard Specification for Aviation Turbine Fuels.*, American Society For Testing and Materials, 2015.

[13] ASTM D7566, *Standard Specification for Aviation Turbine Fuel Containing Synthesized Hydrocarbons*, American Society for Testing and Materials, 2016.

[14] Yarin, A., "DROP IMPACT DYNAMICS: Splashing, Spreading, Receding, Bouncing. . . ," *Annual Review of Fluid Mechanics*, Vol. 38, No. 1, 2006, pp. 159–192. doi:10.1146/annurev.fluid.38.050304.092144.

[15] Ferrao, I., Ribeiro, D., Barata, J. M., and Silva, A. R., "Comparative Study of Droplet Impact onto Sloped Surface versus a Droplet Impact onto a Surface with a Crossflow," *AIAA Scitech 2019 Forum*, American Institute of Aeronautics and Astronautics, 2019. doi:10.2514/6.2019-0629.

[16] Mundo, C., Sommerfeld, M., and Tropea, C., "Droplet-wall interactions: experimental studies of the deformation and breakup process," *International Journal of Multiphase Flow*, Vol. 21, No. 2, 1995, pp. 151–173. doi:10.1016/0301-9322(94)00069-v.

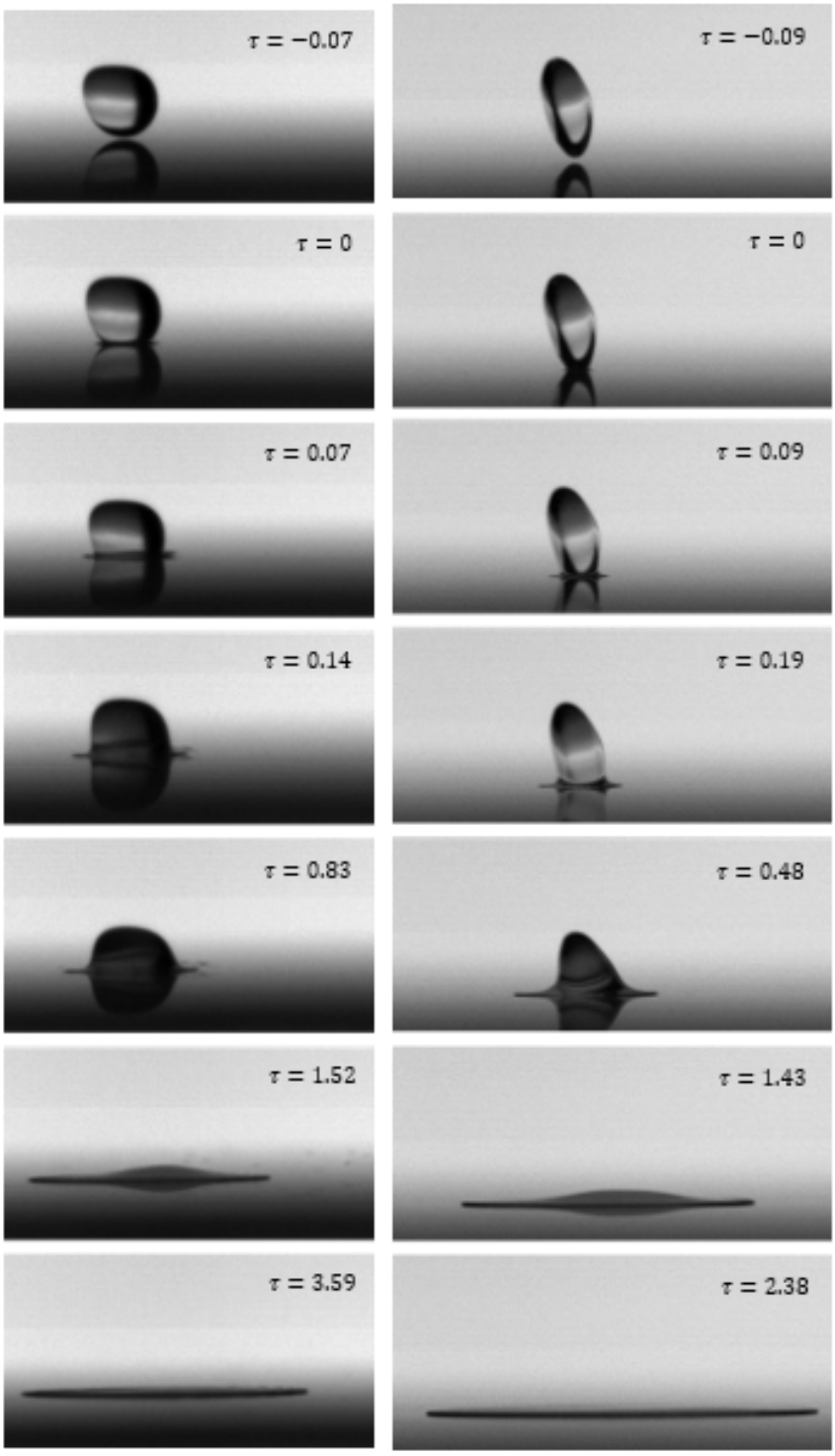

(a) Figure A (b) Figure B

Fig. 1 100% **jet fuel impingement with a crossflow velocity of: a)** $7\,\mathrm{m\,s^{-1}}$ **and b)** $10\,\mathrm{m\,s^{-1}}$**.**

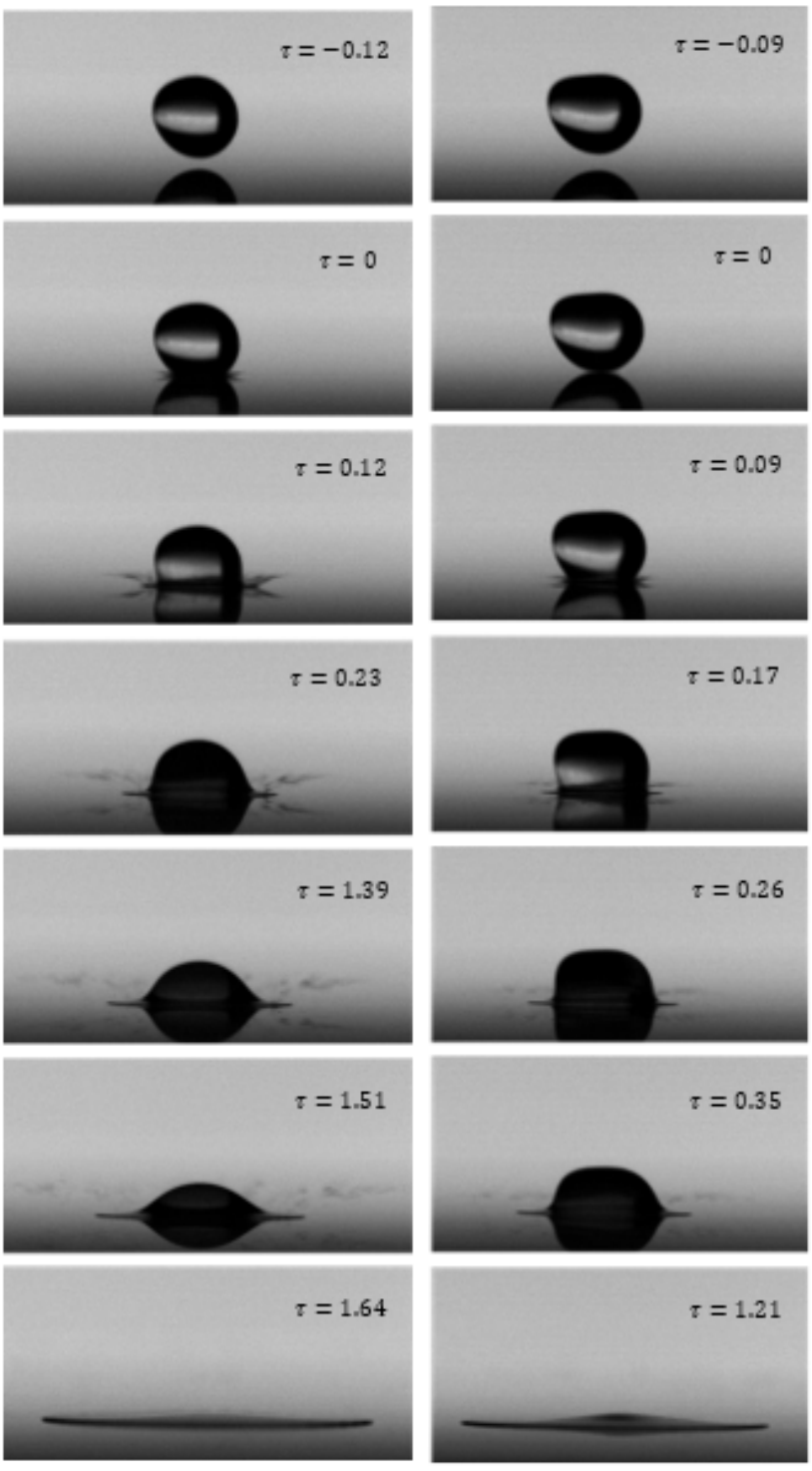

(a) Figure A (b) Figure B

Fig. 2 75% **jet fuel -** 25% **HVO impingement with a crossflow velocity of: a)** $7\,\mathrm{m\,s^{-1}}$ **and b)** $10\,\mathrm{m\,s^{-1}}$**.**

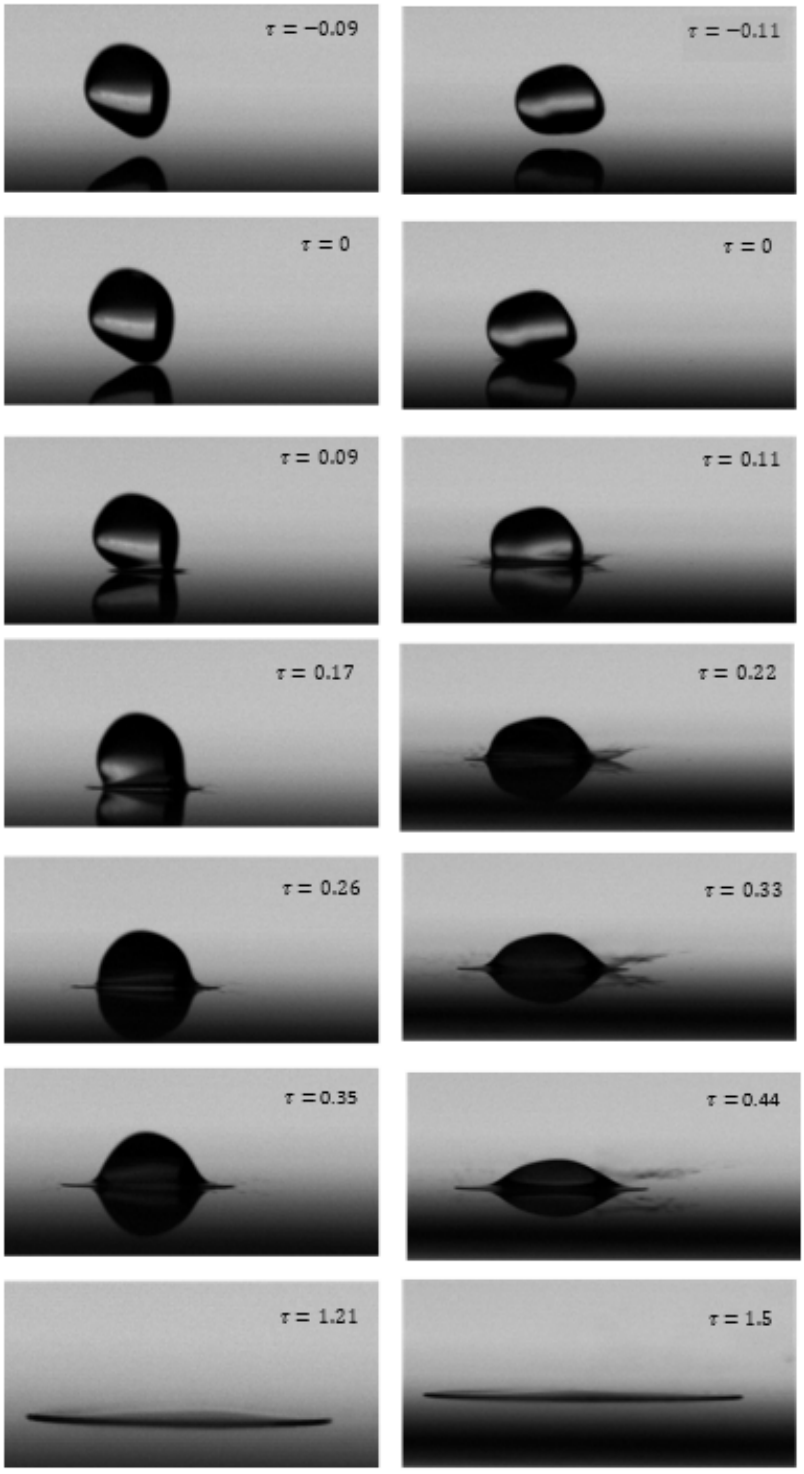

(a) Figure A (b) Figure B

Fig. 3 Outcomes of 75% **jet fuel -** 25% **HVO impingement with a crossflow velocity of** $12\,\mathrm{m\,s^{-1}}$**.**